Title

Proteomic landscape of tunneling nanotubes reveals CD9 and CD81 tetraspanins as key regulators

Roberto Notario Manzano[1,2], Thibault Chaze[3], Eric Rubinstein[4], Mariette Matondo[3], Chiara Zurzolo[1]* & Christel Brou[1]*

[1] Membrane Traffic and Pathogenesis Unit, Department of Cell Biology and Infection, CNRS 18 UMR 3691, Université de Paris, Institut Pasteur, 75015 Paris, France; [2]Sorbonne Université, ED394 - Physiologie, Physiopathologie et Thérapeutique, F-75005 Paris, France; [3]Proteomics Platform, Mass Spectrometry for Biology Unit, CNRS USR 2000, Institut Pasteur, 75015 Paris, France ; [4] Centre d'Immunologie et des Maladies Infectieuses, Inserm, CNRS, Sorbonne Université, CIMI-Paris, 75013 Paris, France

* correspondence : chiara.zurzolo@pasteur.fr; christel.brou@pasteur.fr

Summary

Tunneling nanotubes (TNTs) are open actin- and membrane-based channels, connecting remote cells and allowing direct transfer of cellular material (e.g. vesicles, mRNAs, protein aggregates) from cytoplasm to cytoplasm. Although they are important especially in pathological conditions (e.g., cancers, neurodegenerative diseases), their precise composition and their regulation were still poorly described. Here, using a biochemical approach allowing to separate TNTs from cell bodies and from extracellular vesicles and particles (EVPs), we obtained the full composition of TNTs compared to EVPs. We then focused to two major components of our proteomic data, the CD9 and CD81 tetraspanins, and further investigated their specific roles in TNT formation and function. We show that these two tetraspanins have distinct functions: CD9 participates in the initiation of TNTs, whereas CD81 expression is required to allow the functional transfer of vesicle in the newly formed TNTs, possibly by regulating fusion with the opposing cell.

Introduction

Tunneling nanotubes (TNTs) are thin membranous conduits , supported by F-actin that form continuous cytoplasmic between cells over distances ranging from several hundred nm up to 100 µm [1, 2]. They allow cell-to-cell communication by facilitating the transfer of different cargoes directly from cytoplasm to cytoplasm of the connected cells, including organelles (e.g. lysosomes, mitochondria [3, 4]), micro- or mRNAs, pathogens,

and misfolded/aggregated proteins (e.g., prion proteins, tau or α-synuclein aggregates [5-7]). TNTs could play major roles in various diseases, including neurodegenerative diseases or cancers of different types. In addition to cell cultures and tumors explants [8], TNT-like connections have been shown to exist in the retina and facilitate cellular material transfer between photoreceptors [9, 10] or pericytes [11], highlighting the importance of understanding the biology of these protrusions in order to unravel their possible role(s) *in vivo*. TNT formation is highly dynamic and appears to be regulated by cellular stresses and actin regulators [12]. Two models have been proposed for TNT formation. In the first, TNTs would be produced by membrane deformation and elongation of the protrusion supported by actin polymerization followed by adhesion and fusion of this protrusion with the opposing cell. Alternatively, TNTs could be formed by cell dislodgement where adhesion and membrane fusion would be the first steps before cell bodies separation and elongation of the protrusion by actin polymerization [12, 13]. However, the mechanism(s) and specific pathways governing TNT formation as well as the molecular components of TNTs are still not known.

In addition to TNTs, one of the major pathways used by cells to transfer materials over long distances is through membrane-surrounded vesicles, collectively known as extracellular vesicles (EVs). EVs are released by all cells, and up taken by distant recipient cells [14, 15]. They can be formed either by direct budding from the plasma membrane, or by secretion of intraluminal vesicles of multivesicular compartments (in which case they are called exosomes). Because of their common functions, their similar diameters, and because TNTs are fragile and easily broken and therefore can be released in cell culture supernatants (where EVs are also found), it has been challenging to distinguish TNTs from EVs in terms of composition [16]. In this regard, two members of the tetraspanin family, CD9 and CD81, which are well-known and widely used markers for EVs [17], have been detected in TNTs when overexpressed in T cells [18].

Tetraspanin form a family (with 33 members in mammals) of small four membrane-spanning domain proteins with two extracellular domains, including a large one harboring a tetraspanin-specific folding and two short cytoplasmic tails. Tetraspanins are involved in various cellular processes like migration, adhesion, signaling, pathogen infection, membrane damage reparation, membrane protrusive activity and cell-cell fusion [19-22].

Their function is linked at least in part to their ability to interact with other transmembrane proteins, forming a dynamic network or molecular interactions referred to as the tetraspanin web or Tetraspanin-enriched microdomains (TEM). Inside this "web", the tetraspanins CD9 and CD81 directly interact with the Ig domain proteins CD9P1 (aka EWI-F, encoded by the PTGFRN gene) and EWI-2 (encoded by the IGSF8 gene) [23-26], which have an impact on several fusion processes [27-29]. Whether CD9 and CD81 are also present on TNT from non-T lymphoid cells, and whether they play a role in the formation or function of TNTs has not been investigated.

With the goal of identifying structural components of TNTs, and possibly specific markers and regulators of these structures, we established a protocol of TNT isolation from U2OS cultured cells, allowing to separate TNTs from extracellular vesicles and particles (EVPs) and from cell bodies. We obtained the full composition of TNTs, compared to EVPs. As CD9 and CD81 were major components of TNTs, we further studied their specific roles in TNT formation and ability to transfer cellular material using human neuronal SH-SY5Y, a well known cell model to study functional TNTs. Our data

91 indicate that CD9 and CD81 have different functions and regulate two successive steps
92 of the formation of TNT.
93
94

95 Results

96
97 Purification of TNTs and EVPs
98
99 In order to isolate TNTs, we used U2OS cells because they are robustly adherent cells
100 exhibiting few long protrusions, but are able to grow TNTs and transfer cellular material
101 through these bridges (Figure S1A, B and [30]). Additionally, we took advantage of the
102 fact that TNTs are very sensitive to mechanical stress as they are not attached to
103 substrate [1, 31]. After removal of the cell medium and replacement by a small volume
104 of PBS, the flasks were vigorously shacken in order to break the TNTs that were then
105 isolated from the supernatant by ultracentrifugation after elimination of floating cells
106 by low-speed centrifugations and filtration (see workflow on Figure 1A). When
107 necessary, extracellular vesicles and particles (EVPs) were directly collected from the
108 first cell culture supernatant and enriched following a standardized procedure([17, 32-
109 34] and see Figure 1A).
110 To validate that our protocol for preparing TNTs vs. EVPs was accurate, we sought to
111 engeneer cells with fluorescent TNT markers. As shown in Figure S1A, actin
112 chromobody-GFP (an actin-detecting probe that does not affect actin dynamics [35])
113 decorated TNTs after stable expression. Endogenous CD9 was present on at least a
114 fraction of TNTs formed between U2OS cells, and a GFP-CD9 construct also decorated
115 these structures when stably expressed in these cells (Figure S1B). As a control, cells
116 stably expressing H2B-GFP (labeling nuclei) were used.
117 Four independent preparations of TNTs and EVPs from the same cell cultures (Figure
118 1B), were analyzed. We first validated that the crude preparations (before
119 ultracentrifugation, Figure 1A) contained particles and measured their size and their
120 fluorescence using Nano flow-cytometry. As shown in Figure 1C and S1C-E, both EVPs
121 and TNTs contained particles of similar mean diameter (around 60 nm, Figure S1C, D),
122 ranging from 40 to more than 100nm. The sizes and concentrations of EVPs and TNTs
123 were the same in parental and transfected cell lines (Figure S1D, E). Both preparations
124 contained particles expressing GFP-CD9 (Figure 1C), indicating the presence of
125 membrane-enclosed particles. A major difference between the two preparations was
126 the large fraction of particles in the TNT preparation (38%) that beared the actin
127 chromobody-GFP which was barely detected in EVPs (0.2%). Finally, H2B-GFP was
128 present in a very minor part of the particles, showing that contaminations with cell
129 debris or nuclei were limited, and therefore validating our protocol. Western-blot
130 analysis confirmed such absence of contamination since the Golgi marker GM130 was
131 detected neither in EVP nor in TNT (Figure 1D). CD9 and CD63 were detected in both
132 TNT and EVP preparation, whereas tubulin (shown to partially label TNTs on Figure S1A)
133 was only detected in TNT fraction, which also contained endogenous actin (Figure S1F).
134 Altogether, these data supported that our protocol allowed differential enrichment of
135 the fractions in TNTs and EVPs respectively.
136

137 Analysis of TNTome
138
139 To obtain a full and accurate picture of U2OS TNT content (called TNTome), we made 12
140 independent preparations of TNT fractions (in red in Figure 1A), each starting from about
141 $20x10^6$ cells, and analyzed them by LC-MS/MS. 1177 proteins were identified in at least
142 9 preparations (table S1). We first observed that proteins previously described in TNTs,
143 like actin, Myosin10 [36], ERp29 [30], or N-cadherin [2, 37] were indeed present in
144 TNTome. Less than 100 nuclear proteins, i.e. less than 8% were found (according to GO
145 Cellular component analysis), which could result from partial contamination with
146 cellular debris or dead cells. This is in accordance with nanoFCM results, were H2B-GFP
147 positive particles were 4% of actin-chromobody-GFP positive ones. The 1177 proteins
148 have been ranked in 4 quartiles depending on their relative abundancy (average iBAQ),
149 highlighting the enrichment of specific factors when considering gene ontology (table
150 S1, Figure 2A). These factors could be structural components of TNTs, but also material
151 that was circulating or in the process of being transferred at the time when TNTs were
152 broken and purified. It could be why mitochondrial (8% of the total),
153 lysosomal/endosomal or other vesicle proteins are listed. As highlighted by Proteomap
154 analysis (Figure 2A), TNTome is rich in RNA-associated proteins (ribosomes, translation
155 factors, ribonucleoproteins), in accordance with TNTs being able to transfer micro and
156 mRNAs [38, 39].
157 A major group of proteins of interest were related to cytoskeleton (15%, i.e. 172
158 proteins, see table S2, analysis of GO terms, cellular components). As shown by STRING
159 functional network representation, actin-related proteins were majority (Figure 2B,
160 orange nodes) compared to microtubule-related (green nodes) or intermediate
161 filament-related proteins (blue nodes). This was in accordance with the nature of TNTs,
162 mainly supported by actin cytoskeleton [1]. However, recent work has shown that TNTs,
163 in addition to actin, could contain microtubules as in some cancers (Figure S1A and [8,
164 40]), and also cytokeratins like in the case of urothelial cells [41, 42].
165 When looking at membrane proteins, analysis of the GO terms (cellular components) of
166 the TNTome classified around 500 proteins as membrane-related, 64 of which being
167 strictly integral plasma membrane (see table S3 and Figure 2C). Among the latter, N-
168 cadherin and other cadherin-related proteins (green nodes), as well as known N-
169 cadherin interactors like α-catenin, were found. We also noticed the presence of various
170 integrin subunits (orange nodes, including the Integrin β1, whose presence on TNT was
171 confirmed by immunofluorescence (Figure S2C). However, the TNTome had only a
172 partial overlap with integrin adhesion complexes ([43], Figure S2A and tab1 of table S4)
173 and with the consensus adhesome (Figure S2B, tab2 of table S4). In addition very
174 important proteins of the focal adhesions, like Paxillin, GIT2, Parvins and PINCH1 were
175 not in the TNTome, making unprobable focal adhesion being isolated in TNT
176 preparations. We also analyzed whether TNT preparation could be contaminated by
177 filopodia, another type of protrusions grown by the cells. Despite common proteins
178 described as core filopodia proteins in U2OS cells (like Myosin10, Integrin α5, TLN1,
179 FERMT2, MSN, LIMA1), TNTome was devoid of others (Myo15A, TLN2, PARVA,
180 ITGB1BP1, see [44]), making unlikely an important contamination of TNTs with filopodia
181 during the preparation. Together, these results suggested that the proteins identified in
182 TNTome represent a specific composition of these protrusions, and not a pool of other
183 types of protrusions which could have contaminated the preparation.

184 We also looked whether the TM proteins of the TNTome were the most abundant TM
185 proteins of U2OS cells. We compared the rank in TNTome to the protein concentration
186 [45] or to the level of RNA [46]. Whether some factors are indeed very well expressed
187 in U2OS cells (for instance Integrin β1, SLC3A2, basigin, CLIC channels) and ranked in the
188 first quartile of TNTome, others are weakly expressed in U2OS cells (N-cadherin for
189 instance). In addition, some cell surface proteins are highly expressed in U2OS cells
190 (according to their corresponding RNA level [46]), but not detected in the TNTome, like
191 SLC2A11 (Glucose transporter), APP, ITM2C, TNFR. As shown by WB in Figure S2D, we
192 could detect membrane or membrane-associated proteins in U2OS cell extracts that
193 were not listed in TNTome, like Integrin β4, α4, EGFR, Cx43, and APP [47]. Likewise,
194 some proteins of very low abundancy in cells were found in TNTome (CALML5 for
195 example), maybe reflecting a specific role in TNT formation. We also observed that the
196 relative abundance of some proteins in TNT fractions compared to WCE (Figure S2E) was
197 variable. As examples, CD9 and especially ADAM10 seemed to be relatively abundant in
198 TNTs compared to WCE, whereas Integrin β1 or ANXA2 TNT/WCE ratios were much
199 lower. Altogether, these data suggested that TNT membrane composition was not just
200 a fraction of cell surface membrane proteins, but rather that some proteins were
201 excluded, other more present. This first consolidated our TNT purification procedure,
202 and second highlighted that specific mechanisms and factors should be at stake to grow
203 and maintain TNTs.
204
205 Comparison of the content of TNTs and EVPs
206
207 Because both EVs and TNTs have similar characteristics (membrane-formed, diameter,
208 ability to transfer material to remote cells), we analyzed their respective composition
209 when prepared from the same cell cultures, following the full protocol schematized in
210 Figure 1A, from 4 independent experiments. 961 proteins in total were identified at least
211 in 3 of the 4 TNT and EVP preparations. When keeping TNT proteins that were also
212 present in the 1177 list of TNTome (in 9 TNT preparations over the total of 12), a total
213 of 801 proteins were finally differentially analyzed. Our results showed a different
214 composition of TNTs and EVPs, although common factors represent 75% of them (see
215 volcano plot in Figure 2D). Interestingly, 174 proteins were specific for TNTs when
216 compared to EVPs (see tab1 of table S5). Among the most abundant was the ER
217 chaperone ERp29, previously shown to be required for the formation of TNTs [30]. When
218 discarding organelle-associated or translation linked proteins, 89 proteins remained in
219 this TNT-only list (table S5, tab2, constitutive). 20% of them were involved in
220 cytoskeleton, including the positive regulator of TNTs Myosin10 [36]. When analyzing
221 the proteins differentially abundant in TNT vs. EVPs (Figure 2D and table S6), we noticed
222 the enrichment of TNTs in cytoskeleton-related proteins, especially actin, compared to
223 EVPs.
224 The tetraspanins CD9, CD81 and CD63 are classical markers of EVs and were all detected
225 in TNTs, CD9 and CD81 being among the more abundant transmembrane proteins of
226 TNTome. CD9 and CD63 were more abundant in EVs than in TNT, and CD81 was present
227 at similar level in both preparations. Their direct interacting partners CD9P1 and EWI2
228 (respectively PTGFRN and IGSF8 in Figure 2C) were present in TNTome but more
229 enriched in EVPs than TNTs. Consistent with the presence of the integrins α3β1 and
230 α6β1, the tetraspanin CD151 which directly associates with these integrins was also

231 detected in TNTome [48]. Finally, the presence of CD9, CD81, and CD151 in TNTs was
232 confirmed by immunofluorescence in U2OS (Figures S1A and S2C).
233
234
235 Regulation of TNT formation by CD9 and CD81
236
237 To study the role of CD9 and CD81 in the formation of TNTs, we decided to use a cellular
238 model in which TNT structure and function have already been largely investigated, SH-
239 SY5Y cells. These human neuronal cells form many TNTs (about 30 % of WT cells are
240 connected by TNTs), which are easily visualized and distinguished from other
241 protrusions by fluorescent imaging [2, 7, 49]. Similarly to what we observed in U2OS
242 cells, CD9, CD81 and CD151 were detected on protrusions connecting SH-SY5Y cells
243 (Figure 3A, CD9 in green and CD81 in red, yellow arrowheads indicate TNTs and Figure
244 S2C). Importantly, all protrusions connecting two cells, containing actin and not
245 attached to the substrate, which correspond to TNTs, beared CD9 and CD81, indicating
246 that these tetraspanins are good markers for TNTs.
247 We then knocked-out (KO) CD9 and/or CD81 by infecting SH-SY5Y cells with lentiviral
248 CRISPR vectors targeting the corresponding genes. Western-blot analysis confirmed the
249 lack of CD9 and/or CD81 expression in these cells (Figure S3A). CD9 KO cells, but not
250 CD81 KO cells, showed a significant reduction of the percentage of TNT-connected cells
251 compared to WT cells (Figure 3B&C). The % of TNT-connected cells was even lower in
252 the double KO cells (named CD9&CD81 KO hereafter). The role of CD9 in TNT formation
253 was confirmed by the finding that CD9 stable overexpression (OE) resulted in a
254 significant increase in the % of TNT-connected cells (Figure 3 D&E). Consistently with KO
255 result, CD81 stable OE did not change the % of TNT-connected cells. Together these
256 results showed that CD9 plays a role in the formation or maintenance of TNTs and that
257 CD81 might play a partially redundant role when CD9 is absent.
258
259 Role of CD9 and CD81 in donor cells for TNT function
260
261 The next and complementary step was to evaluate the possible influence of CD9 and
262 CD81 on the functionality of TNTs. TNT functionality is understood as the intrinsic
263 capacity to allow the transfer of different types of cellular material through the open
264 channel formed between the cytoplasm of different cells. This was monitored by
265 quantifying by flow cytometry the transfer of labeled vesicles between two different cell
266 populations (¨donors¨ for the cells where vesicles were first labeled and ¨acceptors¨ for
267 the cells that received the vesicles [50]). A similar gating strategy was applied to all
268 experiments (Figure S4), and the vesicle transfer through any mechanism other than cell
269 contact-dependent was ruled out in all experiments by analyzing secretion controls,
270 where the two cell populations were cultured separately (Figure S5). Therefore, the
271 amount of transferred vesicles occurring mainly through cell-contact-dependent
272 mechanisms is an indirect way of monitoring TNT functionality that has to be analyzed
273 with regard to TNT apparent number.
274 First, we co-cultured WT, CD9 KO, CD81 KO or CD9&CD81 KO donor cells versus WT
275 acceptor cells expressing GFP (as schematized in Figure 3F). Consistently with the
276 decrease of the % of cells connected by TNTs, CD9 KO cells showed a significantly
277 decreased percentage of acceptor cells containing donor's vesicles compared to WT cells

278 (Figures 3F and S4A). On the other hand, despite having no effect on the number of
279 TNTs, CD81 KO caused a significant reduction in vesicle transfer to acceptor cells.
280 CD9&CD81 KO cells showed a further decrease of vesicle transfer, consistent with the
281 high decrease in the % of TNT-connected cells. Next, we performed a co-culture using
282 tetraspanin OE cells as donor cells (Figure 3G). CD9 OE as well as CD81 OE significantly
283 increased vesicle transfer compared to WT cells (Figures 3G and S4B). These data
284 showed that both CD9 and CD81 in donor cells positively regulate the transfer of vesicles
285 through TNTs, which could be in the case of CD9, but not CD81, a direct consequence of
286 an increased number of TNT.
287
288 Pathway of CD9 and CD81 in the regulation of TNTs
289
290 Knowing that the molecular conformation of CD9 molecules can induce membrane
291 curvature [51, 52] and that induced clustering of CD9 can be achieved by treating cells
292 with specific antibodies against this protein [53, 54] that could lead to the formation of
293 protrusions such as microvilli [55], we postulated that CD9 could be involved in the initial
294 steps of formation and asked whether promoting CD9 clustering could affect TNT
295 number and function. Incubation for 2 hours of WT SH-SY5Y cells with an anti-CD9
296 antibody (CD9 AB), but not a control antibody (CTR AB), caused the presence of CD9 in
297 patches on the plasma membrane suggesting that CD9 molecules (and CD81) were
298 incorporated in multimolecular complexes that were clustered together by the
299 antibodies (Figure 4A). Furthermore, the same antibody treatment for an additional 2
300 hours after 24 hours of coculture of WT donor and acceptor cells (Figure 4B) lead to an
301 increase in the % of TNT-connected cells (Figure 4C) that correlated with an increase on
302 the vesicle transfer (Figure 4D). These data suggested that CD9-enriched sites could
303 serve as initiation platforms for TNTs or participate in the stability of these structures.
304 When repeating these experiments on CD81 KO cells, neither CD9 clustering (Figure 4E)
305 nor the increase of TNT number (Figure 4F&G) was affected by the lack of CD81.
306 However, this increase in TNTs was not accompanied by an increase in vesicle transfer
307 (Figure 4H) suggesting that CD9 does not require CD81 to form/stabilize TNTs, but that
308 if CD81 is not present, TNT functionality is compromised.
309 To further understand whether CD9 and CD81 have redundant roles or act successively
310 in the pathway of TNT formation, we knocked-out CD81 in cells over-expressing CD9
311 (Figure S3B). CD9 OE was associated with an increase of the % of TNT-connected cells,
312 which was not changed after CD81 KO (Figure 5 A&B), consistent with the fact that CD81
313 does not play a role in TNT formation, at least in CD9 expressing-cells. However, the
314 transfer from CD9 OE cells was not sentitive to CD81 KO (Figures 5C and S4C), in contrast
315 to WT cells (Figure 3F), suggesting that CD9 OE can compensate for the absence of CD81
316 on vesicle transfer. To determine whether CD81 can replace CD9 in
317 stimulating/stabilizing TNT, we knocked-out CD9 in CD81 OE cells (Figure S3B). As shown
318 in Figure 5B, CD9 KO reduced TNT number to the same extent in these CD81 OE cells
319 than in WT cells (Figure 3C). Consistently with the number of TNTs, the KO of CD9 on
320 CD81 OE cells significantly decreased the transfer compared to CD81 OE cells (Figures
321 5C and S4C). Thus, CD81 cannot compensate for CD9 for the formation/stabilization of
322 TNTs.
323 All the above results pointed out that both CD9 and CD81 participate in the regulation
324 of the TNTs, however not being interchangeable, and are in accordance with CD9 in

325 donor cells acting first in promoting TNT formation, whereas CD81 would act
326 downstream, both events being needed to give full functionality to TNTs.
327
328
329 ## Discussion
330
331 **The composition of TNTs is unique**
332
333 Thanks to a newly established procedure in U2OS cells, we were able to reproducibly
334 isolate a cellular fraction from cell bodies and from EVPs, and analyze their content by
335 mass spectrometry. The physical characteristics as well as the proteome analysis of this
336 fraction (called TNTome) suggested that it could be enriched in TNTs with minor
337 contaminations with other cell protrusions material. Therefore, analysis of the TNTome
338 could give valuable information on core components, traveling material or regulatory
339 factors of TNTs. Our results regarding the unique composition of TNTs were in
340 accordance with those obtained by [16], who used a laser captured microdissection
341 approach combined with mass spectrometry to reveal the composition of various types
342 of cellular protrusions in mouse CAD cells, including growth cones, filopodia and TNTs.
343 Interestingly, among the 190 proteins identified in [16] in 2 samples from hCAD samples
344 (enriched in TNTs), 101 were also found in TNTome (listed in table S7), mostly
345 corresponding to the more abundant cellular proteins. It is possible that laser
346 microdissection allowed a limited amount of material to be purified, and therefore few
347 membrane proteins were identified [16].
348 TNTome is rich in membrane-associated proteins, as well as in proteins linked to the
349 cytoskeleton, in particular related to actin, as it was expected for these structures.
350 TNTome is also abundant in ribonucleoproteins and translation-related factors (220
351 proteins, 19%). Some of them (as well as the proteins identified as nuclear in the
352 databases) could be contaminants coming from cellular debris, however this fraction
353 should not be more than 10% of the total, based on nanoFCM results. Together with the
354 fact that TNTs transfer mitochondria and lysosomes, it is possible that TNTs are used as
355 a route to transfer RNAs alone or tethered to organelles by Annexins (several members
356 in TNTome, including A11), G3BP1 or CAPRIN1 (both in the first quartile of TNTome, [56-
357 58]) or that local translation happens along the TNT to fuel it with required material.
358 Transfer of mRNAs and microRNAs through TNTs has been described [38, 39] and could
359 be one of the major functions of this kind of communication.
360 Regarding membrane, beside tetraspanins, cadherins and integrins, some other plasma
361 membrane TM proteins are of interest. Several amino acids (SLC3A2, SLC1A5 in the first
362 quartile, SLC1A4 and SLC7A1 in the fourth) and monocarboxylate transporters (SLC16A1
363 in the second quartile) were found, suggesting together with the presence of
364 mitochondria and of many metabolic enzymes that active metabolism takes place in
365 TNTs and may be necessary to generate local ATP to power TNT growth [59]. Of note
366 SLC1A5 (Gln transporter ASCT2) and the lactate transporter MCT1 (SLC16A1) have been
367 shown to interact with CD9 in pancreatic cancer stem cells [60] where it promoted their
368 membrane localization and function. This hypothesis will need further investigation.
369 Also, of great interest are SLC1A4 (neutral amino acid transporter) and STX7, which are
370 the only TM proteins uniquely found in TNT and not EVP fraction. As a matter of fact,
371 our results suggested that TNTs are different in composition and maybe regulation from

372 EVPs, although they share numerous factors. Further studying TNT proteins not being
373 present in EVPs will possibly allow to identify TNT specific markers.
374 We focused our attention on tetraspanins CD9 and CD81 to further validate our
375 proteomic approach. Among the structures described to comprise at least one of these
376 factors and that could potentially be contaminants of our TNT preparations, are
377 midbodies. Midbodies have been shown to contain CD9 and its partners CD9-P1 and
378 EWI-2 [61], and these structures could be copurified with TNTs, although in minor
379 amount given the fact that the cells were maintained in serum-free medium for 24 hours
380 before TNTs were harvested. However, no other specific markers of midbodies were
381 detected in our MS data, including CRIK, CEP55, PLK1, PRC1, MKLP1 and 2, although they
382 are expressed in U2OS cells [45, 46]. Of note, only 13 TM proteins are common between
383 TNTome and flemingsome (which has 29), including CD9, CD9P1, EWI2, but also CADHF1
384 and 4, CD44, Integrin α3. Some of these proteins could have a specific role in both TNTs
385 and midbodies, like CD9 and its associated factors. Alternatively, some of these proteins,
386 relatively abundant on plasma membranes, could be randomly present, independently
387 of the specific structure that is analyzed. In any case, TNT and midbodies have different
388 composition.
389 Among the cellular structures that depend on tetraspanin-enriched microdomains are
390 also the recently described migrasomes, which are substrate-attached membrane
391 elongated organelles formed on the branch points or the tips of retraction fibers of
392 migrating cells which allow the release and transfer of cellular material in other cells
393 [62]. Although migrasomes have been described to be enriched in and dependent on
394 tetraspanins-enriched microdomains [63, 64], they are fundamentally different from
395 TNTs since they are attached to the substratum (and probably not collected during the
396 procedure of TNT purification), and exhibit specific markers, identified by MS analysis,
397 which are absent from TNTome (TSPAN 4 and 9, NDST1, PIGK, CPQ, EOGT for example,
398 see 65). Altogether, our TNT purification protocol and proteomic analysis have revealed
399 that TNTs have specific composition, and these data open new avenues to understand
400 how TNTs are formed and regulated.
401
402 **CD9 and CD81 regulate formation of TNTs**
403
404 TNTome in U2OS revealed that CD9 and CD81 are among the most abundant integral
405 membrane proteins in TNTs (see table S3, tab2), and previous results of overexpression
406 [18] and our data showed that they are also present on TNTs in other cell lines, especially
407 SH-SY5Y cells, making them probable compulsory proteins of TNTs. In addition, given
408 the distance between cells connected by TNTs, one can speculate that, under specific
409 signal, one or several membrane proteins would drive growth of TNTs and stimulate
410 actin polymerization, and/or subsequent membrane fusion with the opposing cell. CD9
411 and CD81, as part of TEMs, able to bring together additional proteins, were interesting
412 candidates to fulfill these functions. That is why we have analyzed the ability of the
413 tetraspanins CD9 and CD81 to influence the number of TNTs and their functionality
414 understood as the capacity for cargo transfer between cells in a strict cell contact-
415 dependent manner.
416 Related with the protrusive activity of the membrane and its deformation, which is one
417 mandatory step in the formation of TNTs, the tetraspanins CD9 and CD81 have been
418 shown to induce curvature formation [51, 52] probably because of their inverted cone-

419 like structure. CD9 promotes the formation of digitation junctions [66] and CD81
420 promotes microvilli formation and membrane bending [51]. Our results showed that
421 CD9 is able to increase the % of cells connected by TNTs, therefore CD9 is a positive
422 regulator of TNT biogenesis or of TNT stability. Clustering of CD9 by antibody treatment
423 for a short period of time (2 hours) was more than enough to produce a significant
424 increase in the % of cells connected by TNTs and in the % of acceptor cells that had
425 received vesicles, thus showing that functional TNTs were induced or stabilized.
426 In contrast, OE or KO of CD81 did not affect the % of TNT-connected cells at all, indicating
427 that CD81 does not seem to be involved in the origin of new TNTs. These different roles
428 in the biogenesis of TNTs could be surprising given the strong colocalization of these
429 proteins, and their similar structures [52, 67]. However, although we can see how the
430 single KO of CD9 and CD81 showed different results on the number of TNTs, in the
431 double KO of CD9 and CD81 the % of TNT-connected cells was decreased to even lower
432 levels than in the CD9 KO cells. Therefore, this would indicate that CD9 and CD81 may
433 have partially redundant roles in the biogenesis of TNTs, in accordance also with the
434 partial functional compensation of CD81 KO by CD9 OE. This is reminiscent of their role
435 in oocyte fertilization, with both a complementary effect as CD9-/- CD81-/- mouse
436 oocytes are completely sterile [68, 69], and also partial redundancy as CD81 expression
437 on CD9-/- mouse oocytes restores fertilization in 50% of cases [70].
438 Another fundamental process for the formation of functional TNTs is the fusion of the
439 TNT membrane with the opposing cell to form these open channels [2]. CD9 and CD81
440 have been shown to be positive regulators of sperm-egg fusion [69] and bone marrow
441 macrophage fusion-mediated osteoclast formation in the case of CD9 [71], but negative
442 regulators of cell muscle fusion [27] and multinucleated giant cells formation [72].
443 Therefore, one possibility is that these tetraspanins participate in the fusion of the TNTs
444 with the opposing cell. The co-cultures allowing to quantify the cell contact-dependent
445 transfer of vesicles and therefore the functionality of the TNTs (which is an indirect way
446 of checking whether these structures are in fact open or closed) showed a positive
447 correlation between transfer capacity and number of TNTs when acting on CD9 in donor
448 cells, implying that CD9 is a positive regulator of the whole set of processes of TNT
449 formation. In contrast, CD81 in donor cells positively regulated the functionality of TNTs
450 but not the apparent number of TNTs. Therefore CD81 probably does not play a role in
451 attachment of TNTs to the opposing cell or in TNT stability (in which cases one would
452 expect less TNTs in CD81 KO cells), or in stabilizing active CD9 (we would not see same
453 TNT number and transfer in CD9 OE + CD81 KO conditions as in CD9 OE) but rather favors
454 the fusion of TNTs with the opposing cells.
455
456 **CD9 and CD81 act successively in the formation of TNTs.**
457
458 All these results together show that although CD9 and CD81 regulate the formation of
459 TNTs, their respective role could be at different steps of the whole TNT formation
460 process. CD81 KO in CD9 OE cells had no significant effect on both the % of TNT-
461 connected cells and vesicle transfer compared to CD9 OE cells. In contrast, KO of CD9 on
462 CD81 OE cells resulted in a significant decrease in the % of TNT-connected cells and
463 vesicle transfer compared to CD81 OE alone. These results suggested that CD9 could act
464 early in initiating the formation and allowing CD81 to subsequently participate in the
465 fusion of TNTs with the opposing cell. Furthermore, when we treated CD81 KO cells with

anti-CD9 antibodies, we observed the same increase in TNT number that was seen in WT cells, indicating that the TNT-forming capacity of CD9 is independent of CD81 and was induced by antibody treatment. However, vesicle transfer induction was completely blocked in CD81 KO cells, showing that the first steps of TNT formation were not impaired and that it is instead a late step, probably fusion, that is controlled by CD81. Recent work [64] proposed a role for TEM in forming a rigid ring impairing membrane damage to spread. In a similar way, specific CD9/CD81 TEM could somehow protect membrane around the TNT site where fusion with opposing cell will occur. More work in identifying specific TEM composition in TNTs would be needed to address this hypothesis.

In summary, in this study we have shown that TNTs and EVPs are two cellular structures with partially overlapping composition, and that despite being part of both TNTs and EVPs, the tetraspanins CD9 and CD81 are fundamental regulators of TNT formation with complementary roles in the whole process of biogenesis of these structures. TNTome further analysis will be of great help to identify additional protein, as part of the TEM or not, that could participate in TNT formation and regulation.

Acknowledgements : We acknowledge the Center for Translational Science (CRT)-Cytometry and Biomarkers Unit of Technology and Service (CB UTechS), in particular P.H. Commère. Thanks to Dr. S. Charrin for helpful discussion, Dr. S. Lebreton, Ranabir Chakraborty for critical reading of the manuscript, and all the members of the UTRAF unit for their support. We are grateful for financial support to C.Z. from Institut National du Cancer (PLBIO18-103) and Equipe Fondation Recherche Médicale (FRM EQU202103012692). This work was supported by Equipe Fondation Recherche Médicale (FRM-EQU202103012692), and Agence Nationale de la Recherche (ANR-20-CE13-0032) to C.Z.
Author contributions : Conceptualization: RNM, CB, CZ; methodology: RNM, TC, ER, MM, CB; formal analysis: RNM, TC, CB; writing—original draft: RNM, CB; writing—review and editing: RNM, CB, CZ, ER, TC, MM; funding acquisition: CZ, MM; supervision: CB.

Materials and Methods

Cell lines, lentiviral preparations, plasmids and transfection procedures

U2OS cells were cultured at 37 °C in 5% CO2 in Dulbecco's Modified Eagle's Medium (DMEM + Glutamax, + 4.5 g/l Glucose, + Pyruvate, Gibco), plus 10% fetal calf serum (FCS) and 1% penicillin/streptomycin (P/S). U2OS stably expressing H2B-GFP (Addgene 11680) and actin chromobody GFP (pAC-TagGFP from Chromotek) were obtained by transfection with Fugene HD according to manufacturer’s instructions, followed by sorting of GFP-positive cells. GFP-CD9 expressing U2OS cells were obtained by lentiviral transduction as below, followed by limiting dilution to obtain a clone. SH-SY5Y human neuroblastoma cells were cultured at 37 °C in 5% CO2 in RPMI-1640 (Euroclone), plus 10% FCS and 1% P/S.

512 For the lentiviral preparations, human HEK 293T cells were cultured at 37 °C in 5% CO2 in
513 DMEM (ThermoFisher), with 10% FCS and 1% P/S. Cells were plated one day before
514 transfection at a confluency around 70%. Transfection of the different plasmids was made
515 in a ratio 4:1:4 using lentiviral components pCMVR8,74 (Gag-Pol-Hiv1) and pMDG2 (VSV-
516 G) vectors and the plasmid of interest respectively using FuGENE HD (Promega) according
517 to manufacturer's protocol. CRISPR lentiviral plasmids containing the sequences for CD9:
518 GAATCGGAGCCATAGTCCAA and CD81: AGGAATCCCAGTGCCTGCTG were selected using
519 the CRISPR design tool available at the Broad Institute
520 (https://portals.broadinstitute.org/gpp/public/analysis-tools/sgrna-design). The
521 corresponding guide DNA sequences were cloned into the lentiCRISPRv2 plasmid
522 (#52961; Addgene) according to the instructions of the Zhang laboratory
523 (https://www.addgene.org/52961/). The viral particules were collected and concentrated
524 using LentiX-Concentrator (TakaraBio) after 48 h. To KO CD9 and/or CD81, SH-SY5Y were
525 plated the day before the infection at a confluency of around 70% and next day the
526 lentivirus was added to the cells. 24 hours later the medium with the lentiviruses was
527 removed and cells were selected with RPMI + 1 µg/mL of puromycin for 2 days. After this,
528 cells were splitted 1:5 and reinfected for 24 hours. After these 24 hours, medium was
529 replaced with RPMI + 1 µg/mL of puromycin for 10 days changing the medium every 2-3
530 days. Finally, cells were tested for the absence of expression of CD9 and/or CD81 by
531 western blot (WB).

532 To obtain clones that overexpress CD9 or CD81, SH-SY5Y were plated the day before at a
533 confluency of around 70% and next day cells were transfected with the corresponding
534 plasmid using Lipofectamine 2000 (Invitrogen) following the manufacture
535 recommendations and 72 hours post-transfection cells selected with 350 µg/mL of
536 Hygromicin B (Gibco) for 5 days, changing the medium every 2 days and then with 50
537 µg/mL of Hygromicin B for 10 days more. The CD9 or CD81 OE clones were obtained by
538 limiting dilution and tested for expression of CD9 or CD81 by immunofluorescence and
539 WB.

540 ## TNT and EVP preparation

541 Two million U2OS cells were plated in 75 cm2 flasks for 24 hours, next complete medium
542 was replaced by medium without FCS for an additional 24 hours. For EVP preparation,
543 conditioned medium was collected, centrifugated twice at 2000g to remove cells,
544 concentrated 10-fold on Vivaspin 20 (MWCO 10kD, Cytiva), and next submitted to
545 ultracentrifugation in a Beckman MLS50 rotor at 10,000g for 30 minutes at 4°C.
546 Supernatant was collected and centrifugated at 100,000g for 70 minutes at 4°C,
547 resulting pellet was resuspended in PBS and centrifugated again at 100,000g for 70
548 minutes at 4°C. Pellets were used for Mass Spectrometry, or solubilized in 2x Laemmli
549 for WB analysis.
550 For TNT preparation, cell cultures after removing conditioned medium were washed
551 carefully with PBS, next 2 ml of PBS was added in each flask, which was left on an
552 oscillating shaker for 5 minutes before being shaked (30 sec horizontally, and 4 times 30
553 sec by banging them vigorously). PBS from all flasks was drained, collected and
554 centrifugated twice at 2,000g, and filtered on 0.45 µM syringe filter (Corning) to remove
555 detached cells, next submitted to ultracentrifugation at 100,000g for 70 minutes at 4°C.
556 Pellets were used for Mass Spectrometry or WB. After collecting EVPs and TNTs from

557 cell cultures, cells were harvested in PBS, and cell extracts were prepared in Tris 50 mM
558 pH 7.4, NaCl 300 mM, MgCl2 5 mM, Triton 1% with protease inhibitors (complete mini,
559 Roche).
560

561 ## Nano-Flow Cytometry

562 The size and number of exosomes and TNT particles were identified by Nano-Flow
563 Cytometry (NanoFCM). NanoFCM is applicable when the refractive index of input
564 samples are the same or similar to that of silica particles. The standard working curve of
565 scattering light intensity was established using silica standard sphere. EVPs and TNT
566 particles were isolated from 1 flask of culture following the protocol above except the
567 ultracentrifugation steps. The particle size distribution of samples was measured based
568 on the scattering intensity.
569

570 ## Mass spectrometry

571 Digestion of TNT and EVPs samples

572 Protein pellets were dissolved in urea 8M, Tris 50mM pH 8.0, TCEP (tris(2-
573 carboxyethyl)phosphine) 5mM and SDS (Sodium Dodecyl Sulfate) 2%. SDS was removed
574 using a methanol/ chloroform/ water extraction. Briefly, 3V of ice-cold Methanol was
575 added to the sample then mixed. 2 V of ice-cold chloroform was added and mixed. Then
576 3Vof ice cold water was added and mix. Sample were spinned for 3 min at 5000g at 4°C.
577 Proteins at the organic/inorganic interface were kept and washed 3 times in ice cold
578 methanol. Protein pellet were dissolved in Guanidine 1M, TCEP 5mM, Chloroacetamide
579 20mM, Tris 50mM pH8.0 and samples were heated 5 min at 90°C before digestion in a
580 mix of 500 ng of LysC (Promega) at 37°C for 2h. Dilution with Tris 50mM was done before
581 the addition of trypsin 500 ng (Promega) and digestion at 37°C for 8h. Digestion was
582 stopped by adding 1% final of formic acid. Peptides were purified using a C18 based
583 clean up standard protocol done using Bravo AssayMap device

584 LC-MS/MS analysis of TNT and EVPs.

585 LC-MS/SM analysis of digested peptides was performed on an Orbitrap Q Exactive Plus
586 mass spectrometer (Thermo Fisher Scientific, Bremen) coupled to an EASY-nLC 1200
587 (Thermo Fisher Scientific). A home-made column was used for peptide separation (C_{18}
588 50 cm capillary column picotip silica emitter tip (75 µm diameter filled with 1.9 µm
589 Reprosil-Pur Basic C_{18}-HD resin, (Dr. Maisch GmbH, Ammerbuch-Entringen, Germany)).
590 It was equilibrated and peptide were loaded in solvent A (0.1 % FA) at 900 bars. Peptides
591 were separated at 250 $nl.min^{-1}$. Peptides were eluted using a gradient of solvent B (ACN,
592 0.1 % FA) from 3% to 22% in 140 min, 22% to 42% in 61 min, 42% to 60% in 15 min (total
593 length of the chromatographic run was 240 min including high ACN level step and
594 column regeneration). Mass spectra were acquired in data-dependent acquisition mode
595 with the XCalibur 2.2 software (Thermo Fisher Scientific, Bremen) with automatic
596 switching between MS and MS/MS scans using a top 10 method. MS spectra were
597 acquired at a resolution of 70000 (at *m/z* 400) with a target value of 3×10^6 ions. The
598 scan range was limited from 400 to 1700 *m/z*. Peptide fragmentation was performed
599 using higher-energy collision dissociation (HCD) with the energy set at 26 NCE. Intensity
600 threshold for ions selection was set at 1×10^6 ions with charge exclusion of z = 1 and z >
601 7. The MS/MS spectra were acquired at a resolution of 17500 (at *m/z* 400). Isolation
602 window was set at 2.0 Th. Dynamic exclusion was employed within 35 s.
603

604 All Data were searched using MaxQuant (version 1.6.6.0) using the Andromeda search
605 engine [73] against a human reference proteome (75088 entries, downloaded from
606 Uniprot the 29th of October 2020).
607 The following search parameters were applied: carbamidomethylation of cysteines was
608 set as a fixed modification, oxidation of methionine and protein N-terminal acetylation
609 were set as variable modifications. The mass tolerances in MS and MS/MS were set to 5
610 ppm and 20 ppm respectively. Maximum peptide charge was set to 7 and 5 amino acids
611 were required as minimum peptide length. At least 2 peptides (including 1 unique
612 peptides) were asked to report a protein identification. A false discovery rate of 1% was
613 set up for both protein and peptide levels. iBAQ value was calculated. The match
614 between runs features was allowed for biological replicate only.
615
616 Data analysis
617 Quantitative analysis was based on pairwise comparison of protein intensities. Values
618 were log-transformed (log2). Reverse hits and potential contaminant were removed
619 from the analysis. Proteins with at least 2 peptides were kept for further statistics.
620 Intensity values were normalized by median centering within conditions (normalizeD
621 function of the R package DAPAR [74]). Remaining proteins without any iBAQ value in
622 one of both conditions have been considered as proteins quantitatively present in a
623 condition and absent in the other. They have therefore been set aside and considered
624 as differentially abundant proteins. Next, missing values were imputed using the
625 impute.MLE function of the R package imp4p (https://rdrr.io/cran/imp4p/man/imp4p-
626 package.html). Statistical testing was conducted using a limma t-test thanks to the R
627 package limma [75]. An adaptive Benjamini-Hochberg procedure was applied on the
628 resulting p-values thanks to the function adjust.p of R package cp4p [76] using the
629 robust method described in [77] to estimate the proportion of true null hypotheses
630 among the set of statistical tests. The proteins associated to an adjusted p-value inferior
631 to a FDR level of 1% have been considered as significantly differentially abundant
632 proteins.
633
634 Bioinformatic analysis and data mining
635 Twelve replicates were done for the discovery of TNT proteins. Nine over 12 were kept
636 as being part of the TNT. The 1177 resulting proteins were sorting by quartiles according
637 to their iBAQ value. For each of the 4 lists, proteins composition was depicted using
638 ProteoMap tool [78] to visualize their weighted GO organization and protein
639 contribution for each GO term. Also, a DAVID analysis [79] was done for each quartile
640 of proteins. Functional charts and cluster were used to describe the dataset. Protein
641 networks were visualized using STRING [80] and Cytoscape (cytoscape.org).
642 Resource availability: The mass spectrometry proteomics data have been deposited to
643 the ProteomeXchange Consortium via the PRIDE[1] partner repository with the dataset
644 identifier PXD033089.
645
646 Sample preparation for TNT imaging
647 SH-SY5Y or U2OS-derived cells were trypsinized and counted, and 100,000 or 30,000
648 cells respectively were plated on coverslips. After O/N culture, cells were fixed with
649 specific fixatives to preserve TNT [50], first with Fixative 1 (2% PFA, 0.05%
650 glutaraldehyde and 0.2 M HEPES in PBS) for 15 min at 37 °C, then with fixative 2 (4%

651 PFA and 0.2 M HEPES in PBS) for 15 min at 37 °C . After fixation, cells were washed with
652 PBS and membranes were stained with conjugated wheat germ agglutinin (WGA)-Alexa
653 Fluor (1:300 in PBS, Invitrogen) or Phalloidin-Texas-red (1:300 in PBS, Invitrogen) and
654 DAPI (1:1000) (Invitrogen) at room temperature 15 minutes. After gently washing 3
655 times with PBS, samples were mounted on glass slides with Aqua PolyMount
656 (Polysciences, Inc.). Every different SH-SY5Y cell type (WT, tetraspanin KO or tetraspanin
657 OE) was prepared in the exact same conditions.
658

659 ## Counting or quantification of the % TNT-connected cells (also term as TNT
660 counting or TNT number)

661 With the use of an inverted laser scanning confocal microscope LSM 700 or 900 (Zeiss)
662 controlled by the Zen software (Zeiss) multiple random Z-stack images of different
663 points on the samples were acquired. The images were analyzed according to the
664 morphological criteria of TNTs: structures that connect two distant cells and that are not
665 attached to the substratum. First slices were excluded from the analysis, and only
666 connections in the middle and upper stacks were considered. Cells that have TNTs
667 between them were marked as cells connected by TNTs, and the number of these cells
668 was compared to the total number of cells in the sample, giving the percentage of cells
669 connected by TNTs. The analysis was performed using ICY software
670 (https://icy.bioimageanalysis.org/), by using the "Manual TNT annotation" plugin. In
671 each experiment, at least 200 or more cells were analyzed in every condition. The
672 images were adjusted and processed with the ImageJ (https://imagej.nih.gov/ij/) or Icy
673 softwares.
674

675 ## Co-culture assay (DiD transfer assay) and flow cytometry analysis

676 DiD transfer assays have been described elsewhere [50]. Briefly, the co-culture consisted
677 in two distinctly labeled cell populations: a first population of cells (donors) was treated
678 with Vybrant DiD (dialkylcarbocyanine), a lipophilic dye that stains vesicles, at 1:1000
679 (Thermo Fisher Scientific) in complete medium for 30 min at 37 °C (Life Technologies),
680 the cells were then trypsinized and mixed in a 1:1 ratio with a different cell population
681 (acceptors) of different color to distinguish them from donors (usually expressing GFP)
682 and the co-culture was incubated O/N.
683 In the case of the co-cultures with KO, OE or OE + KO of CD9 and CD81, 400,000 donor
684 cells were mixed with 400,000 acceptor cells on 6-well plates for analysis by flow
685 cytometry. After O/N culture, cells were trypsinized, passed through a cell strainer to
686 dissociate cellular aggregates and fixed with 2% PFA in PBS. Finally, these cells were
687 passed through the CytoFLEX S Flow Cytometer (Beckman Coulter) under the control of
688 the CytoExpert Acquisition software. The data were analyzed with FlowJo software
689 following a similar strategy for all experiments: first the samples were gated to exclude
690 cellular debris by plotting the area obtained with the side scatter (SSC-A) and the area
691 obtained with the forward scatter (FSC-A) obtaining all the cells in the sample. Second,
692 within this previous gate, the sample was gated to exclude cell doublets, plotting the
693 width obtained with side scatter (SSC-W) and the area obtained with forward scatter
694 (FSC-A) thus obtaining the singlets. Finally, within the singlet gate, the co-culture was
695 gated using GFP and DiD expression, resulting in four quadrants delimiting double-
696 negative, GFP-positive, DiD-positive and double-positive populations. The % of acceptor

697 cells receiving DiD-vesicles was obtained by calculating the percentage of acceptor cells
698 with labeled vesicles out of the total number of acceptor cells.
699 In the case of the co-culture of the CD9 AB treatment, 50.000 donor cells were co-
700 cultured with 50.000 acceptor cells on coverslips. Results were analyzed by microscopy
701 as described above, and results were obtained by semi-quantitative analysis using ICY
702 software (http://icy.bioimageanalysis.org/) by calculating the percentage of acceptor
703 cells with labeled vesicles out of the total number of acceptor cells. In each experiment,
704 at least 100 recipient cells per condition were counted. Image montages were built
705 afterward in ImageJ software.
706 In all co-cultures a control of the transfer by secretion was performed. DiD-loaded donor
707 cells were seeded alone (800,000 cells for flow cytometry and 100,000 cells for
708 microscopy) and cultured for 24 hours. Next, the supernatant from these cells was
709 centrifuged and added to the acceptor cells that had been seeded on the previous day
710 under the same conditions as the donors, these acceptor cells were cultured for an
711 additional 24 hours and next fixed and analyzed in the same way as above mentioned.
712

713 ## CD9 antibody (AB) treatment

714 Both TNT counting and vesicle transfer in the CD9 AB treatment were done in the same
715 way as described, with an additional step after 24 hours of coculture consisting in the
716 incubation of the cells with either Goat anti-rabbit Alexa Fluor 305 (Thermofisher ref:
717 A21068-) control antibodies (CTR AB) or anti-CD9 (TS9) antibodies at a concentration of
718 10 µg/µL in RPMI medium without serum or P/S for 2 hours. Subsequently, the cells
719 were fixed and submitted to immunofluorescence. For cells treated with CTR AB, after
720 fixation the cells were incubated with anti-CD9 and anti-CD81 antibodies (as described
721 in the next section). Cells treated with CD9 AB were only further incubated with anti-
722 CD81 antibodies. Results were acquired by confocal microscopy.
723

724 ## Immunofluorescence

725 For immunofluorescence, 100.000 SH-SY5Y cells or 30,000 U2OS cells were seeded on
726 glass coverslips and after O/N culture they were fixed with 4% paraformaldehyde (PFA)
727 for 15 minutes, quenched with 50 mM NH_4Cl for 10 minutes and blocked in 2% BSA in
728 PBS for 20 minutes. Primary antibodies used were: mouse anti-CD9 IgG1 (TS9), anti-
729 CD81 IgG2a (TS81), anti-ITGB1 (β1-vjf, IgG1) or anti-CD151 (TS151, IgG1) were previously
730 described[25], and all of them were used in 2% BSA in PBS during 1 hour. After 3 washes
731 of 10 minutes each with PBS, cells were incubated with each corresponding Alexa Fluor-
732 conjugated secondary antibody (Invitrogen) at 1:1000 in 2% BSA in PBS during 1 hour.
733 Specifically, the secondary antibodies used were: goat anti-mouse with epitope IgG1
734 Alexa Fluor 488 for CD9 (Invitrogen ref: A21121) and goat anti-mouse with epitope IgG2a
735 Alexa Fluor 633 for CD81 (Invitrogen ref: A21136). For the experiments showing the
736 actin cytoskeleton, cells were labeled with Phalloidin- Rhodamine (Invitrogen) in the
737 same mix and conditions as the secondary antibodies. Then, cells were washed 3 times
738 of 10 minutes each with PBS, stained with DAPI and mounted on glass slides with Aqua
739 PolyMount (Polysciences, Inc.). Images were acquired with a confocal microscope
740 LSM700 or 900 (Zeiss) and processed with the ImageJ or Icy softwares.
741

742 ### Western blot
743 For Western blot SH-SY5Y cells were lysed with lysis buffer composed of 150 mM NaCl,
744 5 mM EDTA, 20 mM Tris, pH 8.0, 1% Triton X100 with Roche *cOmplete™* Protease
745 Inhibitor Cocktail. Protein concentration was measured by a Bradford protein assay (Bio-
746 Rad). 20 µg of protein were submitted to PAGE (in non-reducing conditions for
747 tetraspanins and ADAM10) followed by western blot analysis. Primary antibodies used
748 for Western blot were: mouse anti-CD9 IgG1 (TS9, 1:1000), mouse anti-CD81 IgG2a
749 (TS81, 1:1000), mouse anti CD63 (1:1000), mouse anti ADAM10 (11G2, 1:1000)[25, 81],
750 rabbit anti-α-GAPDH (Sigma ref: G9545, 1:1000), rabbit anti-β-actin (Cell Signaling ref:
751 4967, 1:1000), mouse anti-α-tubulin (Sigma ref: T9026, 1:2000), mouse anti-GM130 (BD
752 transduction Laboratories, ref:610822, 1:1000, rabbit ITGB1, ITGB4, ITGA4 (from
753 integrin Ab Sampler kit, Cell signaling ref: 4749, 1:1000), rabbit anti-EGFR (Cell Signaling
754 ref: 4267, 1:1000), rabbit anti-CX43 (Sigma ref: C6219, 1:3000), mouse anti-ANXA2
755 (Proteintech ref: 66035,1:2000).
756 ### Statistical analysis
757 Statistical analysis of experiments concerning the TNT counting and the DiD transfer
758 assay are described elsewhere [4]. Briefly, the statistical tests were applied using either
759 a logistic regression model computed using the 'glm' function of R software
760 (https://www.R-project.org/) or a mixed effect logistic regression model using the lmer
761 and lmerTest R packages, applying a pairwise comparison test between groups.
762 All graphs shown in this study have been made with GraphPad Prism version 9.
763
764

765 ## Bibliography

766 1. Rustom, A., Saffrich, R., Markovic, I., Walther, P., and Gerdes, H.-H. (2004).
767 Nanotubular highways for intercellular organelle transport. Science *303*, 1007–
768 1010. 10.1126/science.1093133.
769 2. Sartori-Rupp, A., Cordero Cervantes, D., Pepe, A., Gousset, K., Delage, E.,
770 Corroyer-Dulmont, S., Schmitt, C., Krijnse-Locker, J., and Zurzolo, C. (2019).
771 Correlative cryo-electron microscopy reveals the structure of TNTs in neuronal
772 cells. Nat Commun *10*, 342. 10.1038/s41467-018-08178-7.
773 3. Abounit, S., Bousset, L., Loria, F., Zhu, S., de Chaumont, F., Pieri, L., Olivo-Marin,
774 J.-C., Melki, R., and Zurzolo, C. (2016). Tunneling nanotubes spread fibrillar α-
775 synuclein by intercellular trafficking of lysosomes. The EMBO Journal *35*, 2120–
776 2138. 10.15252/embj.201593411.
777 4. Pinto, G., Saenz-de-Santa-Maria, I., Chastagner, P., Perthame, E., Delmas, C.,
778 Toulas, C., Moyal-Jonathan-Cohen, E., Brou, C., and Zurzolo, C. (2021). Patient-
779 derived glioblastoma stem cells transfer mitochondria through tunneling
780 nanotubes in tumor organoids. Biochem J *478*, 21–39. 10.1042/BCJ20200710.
781 5. Vargas, J.Y., Loria, F., Wu, Y.-J., Córdova, G., Nonaka, T., Bellow, S., Syan, S.,
782 Hasegawa, M., van Woerden, G.M., Trollet, C., et al. (2019). The Wnt/Ca2+
783 pathway is involved in interneuronal communication mediated by tunneling
784 nanotubes. The EMBO Journal *38*, e101230. 10.15252/embj.2018101230.

6. Dilsizoglu Senol, A., Samarani, M., Syan, S., Guardia, C.M., Nonaka, T., Liv, N., Latour-Lambert, P., Hasegawa, M., Klumperman, J., Bonifacino, J.S., et al. (2021). α-Synuclein fibrils subvert lysosome structure and function for the propagation of protein misfolding between cells through tunneling nanotubes. PLoS Biol *19*, e3001287. 10.1371/journal.pbio.3001287.
7. Chastagner, P., Loria, F., Vargas, J.Y., Tois, J., I Diamond, M., Okafo, G., Brou, C., and Zurzolo, C. (2020). Fate and propagation of endogenously formed Tau aggregates in neuronal cells. EMBO Molecular Medicine *12*, e12025. 10.15252/emmm.202012025.
8. Pinto, G., Brou, C., and Zurzolo, C. (2020). Tunneling Nanotubes: The Fuel of Tumor Progression? Trends in Cancer *6*, 874–888. 10.1016/j.trecan.2020.04.012.
9. Kalargyrou, A.A., Basche, M., Hare, A., West, E.L., Smith, A.J., Ali, R.R., and Pearson, R.A. (2021). Nanotube-like processes facilitate material transfer between photoreceptors. EMBO Rep *22*, e53732. 10.15252/embr.202153732.
10. Ortin-Martinez, A., Yan, N.E., Tsai, E.L.S., Comanita, L., Gurdita, A., Tachibana, N., Liu, Z.C., Lu, S., Dolati, P., Pokrajac, N.T., et al. (2021). Photoreceptor nanotubes mediate the in vivo exchange of intracellular material. The EMBO Journal *40*, e107264. 10.15252/embj.2020107264.
11. Alarcon-Martinez, L., Villafranca-Baughman, D., Quintero, H., Kacerovsky, J.B., Dotigny, F., Murai, K.K., Prat, A., Drapeau, P., and Di Polo, A. (2020). Interpericyte tunnelling nanotubes regulate neurovascular coupling. Nature *585*, 91–95. 10.1038/s41586-020-2589-x.
12. Ljubojevic, N., Henderson, J.M., and Zurzolo, C. (2021). The Ways of Actin: Why Tunneling Nanotubes Are Unique Cell Protrusions. Trends in Cell Biology *31*, 130–142. 10.1016/j.tcb.2020.11.008.
13. Abounit, S., and Zurzolo, C. (2012). Wiring through tunneling nanotubes--from electrical signals to organelle transfer. J Cell Sci *125*, 1089–1098. 10.1242/jcs.083279.
14. Charreau, B. (2021). Secretome and Tunneling Nanotubes: A Multilevel Network for Long Range Intercellular Communication between Endothelial Cells and Distant Cells. International Journal of Molecular Sciences *22*, 7971. 10.3390/ijms22157971.
15. van Niel, G., Carter, D.R.F., Clayton, A., Lambert, D.W., Raposo, G., and Vader, P. (2022). Challenges and directions in studying cell–cell communication by extracellular vesicles. Nat Rev Mol Cell Biol *23*, 369–382. 10.1038/s41580-022-00460-3.
16. Gousset, K., Gordon, A., Kumar Kannan, S., and Tovar, J. (2019). A novel Microproteomic Approach Using Laser Capture Microdissection to Study Cellular Protrusions. International Journal of Molecular Sciences *20*, 1172. 10.3390/ijms20051172.
17. Théry, C., Witwer, K.W., Aikawa, E., Alcaraz, M.J., Anderson, J.D., Andriantsitohaina, R., Antoniou, A., Arab, T., Archer, F., Atkin-Smith, G.K., et al. (2018). Minimal information for studies of extracellular vesicles 2018

829 (MISEV2018): a position statement of the International Society for Extracellular
830 Vesicles and update of the MISEV2014 guidelines. Journal of Extracellular
831 Vesicles *7*, 1535750. 10.1080/20013078.2018.1535750.
832 18. Lachambre, S., Chopard, C., and Beaumelle, B. (2014). Preliminary
833 characterisation of nanotubes connecting T-cells and their use by HIV-1. Biol
834 Cell *106*, 394–404. 10.1111/boc.201400037.
835 19. Charrin, S., le Naour, F., Silvie, O., Milhiet, P.-E., Boucheix, C., and Rubinstein, E.
836 (2009). Lateral organization of membrane proteins: tetraspanins spin their web.
837 Biochem J *420*, 133–154. 10.1042/BJ20082422.
838 20. Charrin, S., Jouannet, S., Boucheix, C., and Rubinstein, E. (2014). Tetraspanins at
839 a glance. J Cell Sci *127*, 3641–3648. 10.1242/jcs.154906.
840 21. Hemler, M.E. (2005). Tetraspanin functions and associated microdomains. Nat
841 Rev Mol Cell Biol *6*, 801–811. 10.1038/nrm1736.
842 22. Huang, Y., and Yu, L. (2022). Tetraspanin-enriched microdomains: The building
843 blocks of migrasomes. Cell Insight *1*, 100003. 10.1016/j.cellin.2021.100003.
844 23. Stipp, C.S., Orlicky, D., and Hemler, M.E. (2001). FPRP, a major, highly
845 stoichiometric, highly specific CD81- and CD9-associated protein. J Biol Chem
846 *276*, 4853–4862. 10.1074/jbc.M009859200.
847 24. Stipp, C.S., Kolesnikova, T.V., and Hemler, M.E. (2001). EWI-2 is a major CD9
848 and CD81 partner and member of a novel Ig protein subfamily. J Biol Chem *276*,
849 40545–40554. 10.1074/jbc.M107338200.
850 25. Charrin, S., Le Naour, F., Oualid, M., Billard, M., Faure, G., Hanash, S.M.,
851 Boucheix, C., and Rubinstein, E. (2001). The major CD9 and CD81 molecular
852 partner. Identification and characterization of the complexes. J Biol Chem *276*,
853 14329–14337. 10.1074/jbc.M011297200.
854 26. Charrin, S., Le Naour, F., Labas, V., Billard, M., Le Caer, J.-P., Emile, J.-F., Petit,
855 M.-A., Boucheix, C., and Rubinstein, E. (2003). EWI-2 is a new component of the
856 tetraspanin web in hepatocytes and lymphoid cells. Biochem J *373*, 409–421.
857 10.1042/BJ20030343.
858 27. Charrin, S., Latil, M., Soave, S., Polesskaya, A., Chrétien, F., Boucheix, C., and
859 Rubinstein, E. (2013). Normal muscle regeneration requires tight control of
860 muscle cell fusion by tetraspanins CD9 and CD81. Nat Commun *4*, 1674.
861 10.1038/ncomms2675.
862 28. Cohen, J., Wang, L., Marques, S., Ialy-Radio, C., Barbaux, S., Lefèvre, B., Gourier,
863 C., and Ziyyat, A. (2022). Oocyte ERM and EWI Proteins Are Involved in Mouse
864 Fertilization. Frontiers in Cell and Developmental Biology *10*.
865 29. Whitaker, E.E., Matheson, N.J., Perlee, S., Munson, P.B., Symeonides, M., and
866 Thali, M. (2019). EWI-2 Inhibits Cell–Cell Fusion at the HIV-1 Virological
867 Presynapse. Viruses *11*, 1082. 10.3390/v11121082.
868 30. Pergu, R., Dagar, S., Kumar, H., Kumar, R., Bhattacharya, J., and Mylavarapu,
869 S.V.S. (2019). The chaperone ERp29 is required for tunneling nanotube
870 formation by stabilizing MSec. Journal of Biological Chemistry *294*, 7177–7193.
871 10.1074/jbc.RA118.005659.

872 31. Pontes, B., Viana, N.B., Campanati, L., Farina, M., Neto, V.M., and Nussenzveig,
873 H.M. (2008). Structure and elastic properties of tunneling nanotubes. Eur
874 Biophys J *37*, 121–129. 10.1007/s00249-007-0184-9.
875 32. Cocozza, F., Grisard, E., Martin-Jaular, L., Mathieu, M., and Théry, C. (2020).
876 SnapShot: Extracellular Vesicles. Cell *182*, 262-262.e1.
877 10.1016/j.cell.2020.04.054.
878 33. Théry, C., Amigorena, S., Raposo, G., and Clayton, A. (2006). Isolation and
879 characterization of exosomes from cell culture supernatants and biological
880 fluids. Curr Protoc Cell Biol *Chapter 3*, Unit 3.22.
881 10.1002/0471143030.cb0322s30.
882 34. Alvarez, M.L., Khosroheidari, M., Kanchi Ravi, R., and DiStefano, J.K. (2012).
883 Comparison of protein, microRNA, and mRNA yields using different methods of
884 urinary exosome isolation for the discovery of kidney disease biomarkers.
885 Kidney International *82*, 1024–1032. 10.1038/ki.2012.256.
886 35. Melak, M., Plessner, M., and Grosse, R. (2017). Actin visualization at a glance.
887 Journal of Cell Science *130*, 525–530. 10.1242/jcs.189068.
888 36. Gousset, K., Marzo, L., Commere, P.-H., and Zurzolo, C. (2013). Myo10 is a key
889 regulator of TNT formation in neuronal cells. Journal of Cell Science *126*, 4424–
890 4435. 10.1242/jcs.129239.
891 37. Chang, M., Lee, O.-C., Bu, G., Oh, J., Yunn, N.-O., Ryu, S.H., Kwon, H.-B.,
892 Kolomeisky, A.B., Shim, S.-H., Doh, J., et al. (2022). Formation of cellular close-
893 ended tunneling nanotubes through mechanical deformation. Sci Adv *8*,
894 eabj3995. 10.1126/sciadv.abj3995.
895 38. Haimovich, G., Dasgupta, S., and Gerst, J.E. (2021). RNA transfer through
896 tunneling nanotubes. Biochem Soc Trans *49*, 145–160. 10.1042/BST20200113.
897 39. Kolba, M.D., Dudka, W., Zaręba-Kozioł, M., Kominek, A., Ronchi, P., Turos, L.,
898 Chroscicki, P., Wlodarczyk, J., Schwab, Y., Klejman, A., et al. (2019). Tunneling
899 nanotube-mediated intercellular vesicle and protein transfer in the stroma-
900 provided imatinib resistance in chronic myeloid leukemia cells. Cell Death Dis
901 *10*, 1–16. 10.1038/s41419-019-2045-8.
902 40. Lou, E. (2020). A Ticket to Ride: The Implications of Direct Intercellular
903 Communication via Tunneling Nanotubes in Peritoneal and Other Invasive
904 Malignancies. Frontiers in Oncology *10*.
905 41. Resnik, N., Prezelj, T., De Luca, G.M.R., Manders, E., Polishchuk, R., Veranič, P.,
906 and Kreft, M.E. (2018). Helical organization of microtubules occurs in a minority
907 of tunneling membrane nanotubes in normal and cancer urothelial cells. Sci
908 Rep *8*, 17133. 10.1038/s41598-018-35370-y.
909 42. Resnik, N., Erman, A., Veranič, P., and Kreft, M.E. (2019). Triple labelling of actin
910 filaments, intermediate filaments and microtubules for broad application in cell
911 biology: uncovering the cytoskeletal composition in tunneling nanotubes.
912 Histochem Cell Biol 152, 311–317. 10.1007/s00418-019-01806-3.
913 43. Horton, E.R., Byron, A., Askari, J.A., Ng, D.H.J., Millon-Frémillon, A., Robertson,
914 J., Koper, E.J., Paul, N.R., Warwood, S., Knight, D., et al. (2015). Definition of a

915 consensus integrin adhesome and its dynamics during adhesion complex
916 assembly and disassembly. Nat Cell Biol *17*, 1577–1587. 10.1038/ncb3257.
917 44. Jacquemet, G., Stubb, A., Saup, R., Miihkinen, M., Kremneva, E., Hamidi, H., and
918 Ivaska, J. (2019). Filopodome Mapping Identifies p130Cas as a
919 Mechanosensitive Regulator of Filopodia Stability. Current Biology *29*, 202-
920 216.e7. 10.1016/j.cub.2018.11.053.
921 45. Beck, M., Schmidt, A., Malmstroem, J., Claassen, M., Ori, A., Szymborska, A.,
922 Herzog, F., Rinner, O., Ellenberg, J., and Aebersold, R. (2011). The quantitative
923 proteome of a human cell line. Molecular Systems Biology *7*, 549.
924 10.1038/msb.2011.82.
925 46. Lundberg, E., Fagerberg, L., Klevebring, D., Matic, I., Geiger, T., Cox, J., Algenäs,
926 C., Lundeberg, J., Mann, M., and Uhlen, M. (2010). Defining the transcriptome
927 and proteome in three functionally different human cell lines. Mol Syst Biol *6*,
928 450. 10.1038/msb.2010.106.
929 47. Jouannet, S., Saint-Pol, J., Fernandez, L., Nguyen, V., Charrin, S., Boucheix, C.,
930 Brou, C., Milhiet, P.-E., and Rubinstein, E. (2016). TspanC8 tetraspanins
931 differentially regulate the cleavage of ADAM10 substrates, Notch activation
932 and ADAM10 membrane compartmentalization. Cell Mol Life Sci *73*, 1895–
933 1915. 10.1007/s00018-015-2111-z.
934 48. Boucheix, C., and Rubinstein, E. (2001). Tetraspanins. Cell Mol Life Sci *58*, 1189–
935 1205. 10.1007/PL00000933.
936 49. Pepe, A., Pietropaoli, S., Vos, M., Barba-Spaeth, G., and Zurzolo, C. (2022).
937 Tunneling nanotubes provide a route for SARS-CoV-2 spreading. Sci Adv *8*,
938 eabo0171. 10.1126/sciadv.abo0171.
939 50. Abounit, S., Delage, E., and Zurzolo, C. (2015). Identification and
940 Characterization of Tunneling Nanotubes for Intercellular Trafficking. Current
941 Protocols in Cell Biology *67*, 12.10.1-12.10.21.
942 10.1002/0471143030.cb1210s67.
943 51. Bari, R., Guo, Q., Xia, B., Zhang, Y.H., Giesert, E.E., Levy, S., Zheng, J.J., and
944 Zhang, X.A. (2011). Tetraspanins regulate the protrusive activities of cell
945 membrane. Biochemical and Biophysical Research Communications *415*, 619–
946 626. 10.1016/j.bbrc.2011.10.121.
947 52. Umeda, R., Satouh, Y., Takemoto, M., Nakada-Nakura, Y., Liu, K., Yokoyama, T.,
948 Shirouzu, M., Iwata, S., Nomura, N., Sato, K., et al. (2020). Structural insights
949 into tetraspanin CD9 function. Nat Commun *11*, 1606. 10.1038/s41467-020-
950 15459-7.
951 53. Nydegger, S., Khurana, S., Krementsov, D.N., Foti, M., and Thali, M. (2006).
952 Mapping of tetraspanin-enriched microdomains that can function as gateways
953 for HIV-1. Journal of Cell Biology *173*, 795–807. 10.1083/jcb.200508165.
954 54. Khurana, S., Krementsov, D.N., de Parseval, A., Elder, J.H., Foti, M., and Thali,
955 M. (2007). Human Immunodeficiency Virus Type 1 and Influenza Virus Exit via
956 Different Membrane Microdomains. J Virol *81*, 12630–12640.
957 10.1128/JVI.01255-07.

958 55. Singethan, K., Müller, N., Schubert, S., Lüttge, D., Krementsov, D.N., Khurana,
959 S.R., Krohne, G., Schneider-Schaulies, S., Thali, M., and Schneider-Schaulies, J.
960 (2008). CD9 Clustering and Formation of Microvilli Zippers Between Contacting
961 Cells Regulates Virus-Induced Cell Fusion. Traffic 9, 924–935. 10.1111/j.1600-
962 0854.2008.00737.x.
963 56. Liao, Y.-C., Fernandopulle, M.S., Wang, G., Choi, H., Hao, L., Drerup, C.M., Patel,
964 R., Qamar, S., Nixon-Abell, J., Shen, Y., et al. (2019). RNA Granules Hitchhike on
965 Lysosomes for Long-Distance Transport, Using Annexin A11 as a Molecular
966 Tether. Cell *179*, 147-164.e20. 10.1016/j.cell.2019.08.050.
967 57. Lesnik, C., Golani-Armon, A., and Arava, Y. (2015). Localized translation near the
968 mitochondrial outer membrane: An update. RNA Biology *12*, 801–809.
969 10.1080/15476286.2015.1058686.
970 58. Cioni, J.-M., Lin, J.Q., Holtermann, A.V., Koppers, M., Jakobs, M.A.H., Azizi, A.,
971 Turner-Bridger, B., Shigeoka, T., Franze, K., Harris, W.A., et al. (2019). Late
972 Endosomes Act as mRNA Translation Platforms and Sustain Mitochondria in
973 Axons. Cell *176*, 56-72.e15. 10.1016/j.cell.2018.11.030.
974 59. Garde, A., Kenny, I.W., Kelley, L.C., Chi, Q., Mutlu, A.S., Wang, M.C., and
975 Sherwood, D.R. (2022). Localized glucose import, glycolytic processing, and
976 mitochondria generate a focused ATP burst to power basement-membrane
977 invasion. Developmental Cell *57*, 732-749.e7. 10.1016/j.devcel.2022.02.019.
978 60. Wang, V.M.-Y., Ferreira, R.M.M., Almagro, J., Evan, T., Legrave, N., Zaw Thin,
979 M., Frith, D., Carvalho, J., Barry, D.J., Snijders, A.P., et al. (2019). CD9 identifies
980 pancreatic cancer stem cells and modulates glutamine metabolism to fuel
981 tumour growth. Nat Cell Biol *21*, 1425–1435. 10.1038/s41556-019-0407-1.
982 61. Addi, C., Presle, A., Frémont, S., Cuvelier, F., Rocancourt, M., Milin, F., Schmutz,
983 S., Chamot-Rooke, J., Douché, T., Duchateau, M., et al. (2020). The
984 Flemmingsome reveals an ESCRT-to-membrane coupling via
985 ALIX/syntenin/syndecan-4 required for completion of cytokinesis. Nat Commun
986 *11*, 1941. 10.1038/s41467-020-15205-z.
987 62. Ma, L., Li, Y., Peng, J., Wu, D., Zhao, X., Cui, Y., Chen, L., Yan, X., Du, Y., and Yu,
988 L. (2015). Discovery of the migrasome, an organelle mediating release of
989 cytoplasmic contents during cell migration. Cell Res *25*, 24–38.
990 10.1038/cr.2014.135.
991 63. Huang, Y., Zucker, B., Zhang, S., Elias, S., Zhu, Y., Chen, H., Ding, T., Li, Y., Sun, Y.,
992 Lou, J., et al. (2019). Migrasome formation is mediated by assembly of micron-
993 scale tetraspanin macrodomains. Nat Cell Biol *21*, 991–1002. 10.1038/s41556-
994 019-0367-5.
995 64. Huang, Y., Zhang, X., Wang, H.-W., and Yu, L. (2022). Assembly of Tetraspanin-
996 enriched macrodomains contains membrane damage to facilitate repair. Nat
997 Cell Biol *24*, 825–832. 10.1038/s41556-022-00920-0.
998 65. Zhao, X., Lei, Y., Zheng, J., Peng, J., Li, Y., Yu, L., and Chen, Y. (2019).
999 Identification of markers for migrasome detection. Cell Discov *5*, 1–4.
1000 10.1038/s41421-019-0093-y.

1001 66. Huang, C., Fu, C., Wren, J.D., Wang, X., Zhang, F., Zhang, Y.H., Connel, S.A.,
1002 Chen, T., and Zhang, X.A. (2018). Tetraspanin-enriched Microdomains Regulate
1003 Digitation Junctions. Cell Mol Life Sci 75, 3423–3439. 10.1007/s00018-018-
1004 2803-2.
1005 67. Zimmerman, B., Kelly, B., McMillan, B.J., Seegar, T.C.M., Dror, R.O., Kruse, A.C.,
1006 and Blacklow, S.C. (2016). Crystal Structure of a Full-Length Human Tetraspanin
1007 Reveals a Cholesterol-Binding Pocket. Cell *167*, 1041-1051.e11.
1008 10.1016/j.cell.2016.09.056.
1009 68. Rubinstein, E., Ziyyat, A., Prenant, M., Wrobel, E., Wolf, J.-P., Levy, S., Le Naour,
1010 F., and Boucheix, C. (2006). Reduced fertility of female mice lacking CD81.
1011 Developmental Biology *290*, 351–358. 10.1016/j.ydbio.2005.11.031.
1012 69. Rubinstein, E., Ziyyat, A., Wolf, J.-P., Le Naour, F., and Boucheix, C. (2006). The
1013 molecular players of sperm–egg fusion in mammals. Seminars in Cell &
1014 Developmental Biology *17*, 254–263. 10.1016/j.semcdb.2006.02.012.
1015 70. Kaji, K., Oda, S., Miyazaki, S., and Kudo, A. (2002). Infertility of CD9-Deficient
1016 Mouse Eggs Is Reversed by Mouse CD9, Human CD9, or Mouse CD81;
1017 Polyadenylated mRNA Injection Developed for Molecular Analysis of Sperm–
1018 Egg Fusion. Developmental Biology *247*, 327–334. 10.1006/dbio.2002.0694.
1019 71. Ishii, M., Iwai, K., Koike, M., Ohshima, S., Kudo-Tanaka, E., Ishii, T., Mima, T.,
1020 Katada, Y., Miyatake, K., Uchiyama, Y., et al. (2006). RANKL-Induced Expression
1021 of Tetraspanin CD9 in Lipid Raft Membrane Microdomain Is Essential for Cell
1022 Fusion During Osteoclastogenesis. Journal of Bone and Mineral Research *21*,
1023 965–976. 10.1359/jbmr.060308.
1024 72. Takeda, Y., Tachibana, I., Miyado, K., Kobayashi, M., Miyazaki, T., Funakoshi, T.,
1025 Kimura, H., Yamane, H., Saito, Y., Goto, H., et al. (2003). Tetraspanins CD9 and
1026 CD81 function to prevent the fusion of mononuclear phagocytes. Journal of Cell
1027 Biology *161*, 945–956. 10.1083/jcb.200212031.
1028 73. Tyanova, S., Temu, T., and Cox, J. (2016). The MaxQuant computational
1029 platform for mass spectrometry-based shotgun proteomics. Nat Protoc *11*,
1030 2301–2319. 10.1038/nprot.2016.136.
1031 74. Wieczorek, S., Combes, F., Lazar, C., Giai Gianetto, Q., Gatto, L., Dorffer, A.,
1032 Hesse, A.-M., Couté, Y., Ferro, M., Bruley, C., et al. (2017). DAPAR & ProStaR:
1033 software to perform statistical analyses in quantitative discovery proteomics.
1034 Bioinformatics *33*, 135–136. 10.1093/bioinformatics/btw580.
1035 75. Pounds, S., and Cheng, C. (2006). Robust estimation of the false discovery rate.
1036 Bioinformatics *22*, 1979–1987. 10.1093/bioinformatics/btl328.
1037 76. Smyth, G.K. (2004). Linear Models and Empirical Bayes Methods for Assessing
1038 Differential Expression in Microarray Experiments. Statistical Applications in
1039 Genetics and Molecular Biology *3*. 10.2202/1544-6115.1027.
1040 77. Giai Gianetto, Q., Combes, F., Ramus, C., Bruley, C., Couté, Y., and Burger, T.
1041 (2016). Calibration plot for proteomics: A graphical tool to visually check the
1042 assumptions underlying FDR control in quantitative experiments. PROTEOMICS
1043 *16*, 29–32. 10.1002/pmic.201500189.

1044 78. Liebermeister, W., Noor, E., Flamholz, A., Davidi, D., Bernhardt, J., and Milo, R.
1045 (2014). Visual account of protein investment in cellular functions. Proceedings
1046 of the National Academy of Sciences *111*, 8488–8493.
1047 10.1073/pnas.1314810111.
1048 79. Sherman, B.T., Hao, M., Qiu, J., Jiao, X., Baseler, M.W., Lane, H.C., Imamichi, T.,
1049 and Chang, W. (2022). DAVID: a web server for functional enrichment analysis
1050 and functional annotation of gene lists (2021 update). Nucleic Acids Research
1051 *50*, W216–W221. 10.1093/nar/gkac194.
1052 80. Szklarczyk, D., Gable, A.L., Nastou, K.C., Lyon, D., Kirsch, R., Pyysalo, S.,
1053 Doncheva, N.T., Legeay, M., Fang, T., Bork, P., et al. (2021). The STRING
1054 database in 2021: customizable protein-protein networks, and functional
1055 characterization of user-uploaded gene/measurement sets. Nucleic Acids Res
1056 *49*, D605–D612. 10.1093/nar/gkaa1074.
1057 81. Arduise, C., Abache, T., Li, L., Billard, M., Chabanon, A., Ludwig, A., Mauduit, P.,
1058 Boucheix, C., Rubinstein, E., and Naour, F.L. (2008). Tetraspanins Regulate
1059 ADAM10-Mediated Cleavage of TNF-α and Epidermal Growth Factor. The
1060 Journal of Immunology *181*, 7002–7013. 10.4049/jimmunol.181.10.7002.

1061
1062

1063 Figure legends

1064

1065 Figure 1: Validation of the purification procedures

1066 A. Workflow for TNT vs. EVP purification. EVPs were purified from cell culture
1067 supernatant, TNTs from remaining attached cell supernatant after shaking.
1068 *indicates the fraction used for nanoFCM analysis.
1069 B. Schematic representation of stable cell lines where green color indicates the
1070 location of GFP-tagged protein: H2B-GFP (nuclear), actin chromobody-GFP (actin
1071 cytoskeleton including TNTs) and GFP-CD9 (cell surface, TNTs, EVPs).
1072 C. Scatter dot plot representing the mean percentage (with SD) of GFP-positive
1073 particles analyzed by nanoFCM. Statistical analysis of 4 independent
1074 experiments (6 for GFP-CD9, oneway Anova with Tukey post hoc correction)
1075 show the following respective p-values (from top): blue*: 0.0252, red**: 0.0089,
1076 red*: 0.0131, black*: 0.0161. Means values are (from left to right): 0.01, 0.3, 4.8,
1077 1.75, 0.17, 37.07, 27.7 and 11.6.
1078 D. Western blot of WCE (20µg, corresponding to around $0.1x10^6$ cells), TNT and EVP
1079 fractions (both from 10 10^6 cells) prepared from the same cells, blotted with CD9,
1080 α-tubulin and GM130 specific antibodies. White lane indicates that intervening
1081 lanes of the same gel (and same exposure) have been spliced out.
1082

1083 Figure 2: Analysis of the TNTome

1084 A. Proteomap of the 1177 proteins of the TNTome, sorted in 4 quartiles depending
1085 on their mean iBAQ. Protein accession and mean iBAQ was used to create
1086 ProteoMap, analyzed according to Gene Ontology.

1087 B. STRING physical association network for the cytoskeleton-related proteins listed
1088 in table S2. Color groups were created using Cytoscape. Green are microtubule-
1089 related proteins, blue are intermediate filaments, orange are actin-interacting
1090 proteins. Blue and pink edges show physical interactions based on databases and
1091 experiments respectively.
1092 C. Full STRING functional association network for integral surface membrane
1093 proteins of TNTome, based on table S3. Orange are Integrin proteins, red are
1094 Ephrin receptors, dark green are Cadherins, light green are Sodium/potassium
1095 transporting ATPase ions channels, purple are monocarboxylate and amino acids
1096 transporters, and yellow are tetraspanin-related proteins.
1097 D. Volcano plot of the mass spectrometry analysis based on the 4 EVP and TNT
1098 preparations, showing the maximum log2(Fold-change) in x-axis measured
1099 between TNT and EVP fractions and the corresponding -log10 (p-value) in y-axis.
1100 Dashed lines indicate differential analysis quadrants with log2 (Fold-change)
1101 =0.58 and false discovery rate FDR = 1%. Common EVP=TNT are non-significantly
1102 different (FDR >0.05) with FC>1.5, and FC<1.5. Each quadrant is named above
1103 and the number of identified proteins is indicated. Left and right are proteins
1104 non overlapping in both fractions: TNT-only and EVP only. Note that in EVP-only
1105 fraction, 10 proteins were found in TNTome (based on 12 experiments) and
1106 should therefore be removed. For the TNT proteins, only the proteins also
1107 present in TNTome have been counted.
1108
1109 Figure 3: Expression of CD9/CD81 in TNTs and effects of their overexpression or
1110 invalidation
1111 A. Immunofluorescence of CD9 (green) and CD81 (red) in SH-SY5Y cells. Cells were
1112 also stained with phalloidin (magenta) and DAPI (blue) to visualize actin and
1113 nuclei. This representative image corresponds to the 4th to 5th slices of a stack
1114 comprising 11 slices (1 being at the bottom).
1115 B. Representative images of TNT-connected cells in WT, CD9 KO, CD81 KO and
1116 CD9&CD81 KO cells, stained with WGA-488 (green) to label the membrane and
1117 DAPI (blue) to label the nuclei.
1118 C. Graph of the % of TNT-connected cells in the different cells, from 3 independent
1119 experiments. Mean and standard deviation (SD) are: WT = 31.6 ± 1.25; CD9 KO =
1120 25.2 ± 1.24; CD81 KO = 30.4 ± 1.65; CD9 & CD81 KO = 16.3 ± 4.81. p-values are
1121 indicated above the brackets in all graphs.
1122 D. Representative images of TNT-connected cells in WT, CD9 OE and CD81 OE cells,
1123 stained as in B. Yellow arrowheads show TNTs and scale bars correspond to 10
1124 µm in A, B and D.
1125 E. Graph of the % of TNT-connected cells in the indicated cells from 3 independent
1126 experiments. Mean ± SD are: WT = 29.8 ± 1.11; CD9 OE = 45.3 ± 3.17; CD81 OE =
1127 29.5 ± 0.84.
1128 F. Vesicle transfer assay from donor cells KO of CD9 and CD81, as schematized on
1129 the left. Graphs are % of acceptor cells containing DiD vesicles from 3
1130 independent experiments. Mean ± SD are: WT = 32.7 ± 10.25; CD9 KO = 18.4 ± 8;
1131 CD81 KO = 19.1 ± 4.86; CD9 & CD81 KO = 10.5 ± 1.52.
1132 G. Vesicle transfer assay from donor cells OE CD9 or CD81, as schematized on the
1133 left. Graphs are % of acceptor cells containing DiD vesicles from 3 independent

experiments. Mean ± SD are: WT = 29.3 ± 7.45; CD9 OE = 61.3 ± 20.44; CD81 OE = 55.6 ± 10.31.

Figure 4: CD9 antibody treatment in WT and CD81 KO cells

A. Immunofluorescence of CD9 (green) and CD81 (red) in SH-SY5Y WT cells treated with control antibodies (CTR AB) or with antibodies anti-CD9 (CD9 AB) for 2 hours followed by PFA fixation and incubation with anti-CD81 (for CD9 AB samples) or anti-CD81 + anti-CD9 (for CTR AB samples) and appropriate fluorescent secondary antibodies. This representative image corresponds to the 3th to 4th slices of a stack comprising 12 slices for CTR AB and to the 3th to 4th slices of a stack comprising 11 slices for CD9 AB. Cells were also stained with phalloidin (magenta) and DAPI (blue) to visualize actin and nuclei respectively. The scale bars correspond to 10 µm.
B. Schematic of the antibody treatment experiment. Coculture of WT SH-SY5Y donor cells (DiD in yellow circles to stain the vesicles) and WT GFP-labeled acceptor cells were treated with control antibodies (CTR AB) or with antibodies anti-CD9 (CD9 AB) for an additional 2 hours.
C. Graph of the % of TNT-connected cells in CTR AB or CD9 AB treatment in WT cells. Mean ± SD (N=3) are: CTR AB = 28.8 ± 1.32; CD9 AB = 37.4 ± 0.80.
D. Graph of the % of acceptor cells containing DiD vesicles of the cocultures of WT cells with CTR AB or CD9 AB treatment. Mean ± SD (N=3) are: CTR AB = 27.7 ± 2.48; CD9 AB = 36.8 ± 3.03.
E. Immunofluorescence of CD9 (green) in SH-SY5Y CD81 KO cells treated with control antibodies (CTR AB) or with antibodies anti-CD9 (CD9 AB) for 2 hours followed by PFA fixation and incubation with anti-CD9 (for CTR AB samples) and appropriate fluorescent secondary antibodies. This representative image corresponds to the 3th to 4th slices of a stack comprising 10 slices for CTR AB and to the 5th to 6th slices of a stack comprising 12 slices for CD9 AB. Cells were also stained with phalloidin (magenta) and DAPI (blue) to visualize actin and nuclei respectively. Scale bars are 10 µm.
F. Schematic showing the coculture strategy adapted from B to the antibody treatment in SH-SY5Y CD81 KO cells.
G. Graph of the % of TNT-connected cells in the coculture and antibody treatment described in F. Mean ± SD (N=3): CTR AB = 28.8 ± 0.68; CD9 AB = 43 ± 2.23.
H. Graph of the % of acceptor cells containing DiD vesicles of the experiment schematized in F. Mean ± SD (N=3): CTR AB = 20.6 ± 1.67; CD9 AB = 20.6 ± 2.16

Figure 5: CD9 and CD81 act successively in the formation of TNTs

A. Representative images of WT, CD9 OE, CD9 OE + CD81 KO, CD81 OE and CD81 OE + CD9 KO cells, stained with WGA-488 (green) and DAPI (blue). Yellow arrowheads show TNTs. Scale bars correspond to 10 µm.
B. Graph of the % of TNT-connected cells in the tetraspanin OE + KO cells. Mean ± SD (N=3) are: WT = 28.6 ± 2.05; CD9 OE = 44.2 ± 2.4; CD9 OE + CD81 KO = 48.2 ± 2.16; CD81 OE = 29.5 ± 1.36; CD81 OE + CD9 KO = 20.2 ± 2.09. p-values are above the brackets.

C. Coculture between tetraspanin OE + KO cells used as donors and WT GFP cells used as acceptors, as schematized on the left. The graph shows the % of acceptor cells containing DiD vesicles. Mean ± SD from 3 independent experiments: WT = 26.1 ± 8.94; CD9 OE = 73.8 ± 12.64; CD9 OE + CD81 KO = 87.7 ± 5.11; CD81 OE = 73 ± 14.60; CD81 OE + CD9 KO = 45.4 ± 11.53.

Supplementary tables:

Table S1: the full TNTome (1177 proteins), from 12 independent samples, proteins were conserved when present in more than 9 replicats, ranked in 4 quartiles (from higher to lower mean iBAQ) represented in different colors (orange Q1, green Q2, pink Q3, blue Q4). iBAQ of each sample is indicated for each protein.

Table S2: Cytoskeleton-associated proteins of the TNTome. Proteins identified by GO term analysis (cellular components), except those associated to proteasome, RNA and mitochondria, are ranked according to their quartile assignement (orange Q1, green Q2, pink Q3, blue Q4).

Table S3: Membrane-related proteins identified by GO term analysis (cellular components). Mitochondrial and other organelles membrane proteins have been discarded from GO analysis. Tab 1 lists all membrane and membrane-associated proteins, tab 2 only the integral membrane proteins, ranked according to their quartile assignement (orange Q1, green Q2, pink Q3, blue Q4) and from more abundant to less abundant. Integrins, Ephrin receptors, Cadherins and tetraspanin-related proteins are highlighted respectively in orange, red, dark gree and yellow as indicated in tab2.

Table S4: comparison of TNTome and Integrin adhesion complexes
Tab1 shows the common elements in integrin adhesion complexes (2240 proteins according to Horton et al, 2015) and in TNTome: 765 proteins listed in alphabetical order of the gene name (yellow background). On the right (blue background) are the 413 elements included exclusively in TNTome. Tab2 shows the 26 common elements in consensus adhesome (Horton 2015) and TNTome.

Table S5: TNT-only proteins
Tab1 (total) shows the 174 proteins present in TNT preparations and absent from EVPs. Tab2 (constitutive) shows the 89 TNT-only proteins without proteins described as mitochondrial, nuclear, ER or RNA-related. In yellow background are cytoskeleton-related proteins (20%).

Table S6: overlapping proteins between TNTs and EVPs
Tab1 (TOT TNT>EVP) shows the proteins more abundant in TNTs compared to EVPs, cleaned of nuclear, mitochondrial or RNA-related described proteins in tab2 (TNT>EVP). In yellow background are cytoskeleton-related proteins (29%).

Table S7: Common proteins between TNTome and protrusions from hCAD cells described in *Gousset et al., 2019*. The 190 proteins present in 2 samples of hCAD (mouse

1227 CAD cells treated with H2O2) were converted to their human ortholog, next compared
1228 to the 1177 proteins of table S1.
1229
1230
1231
1232
1233
1234

Figure 1

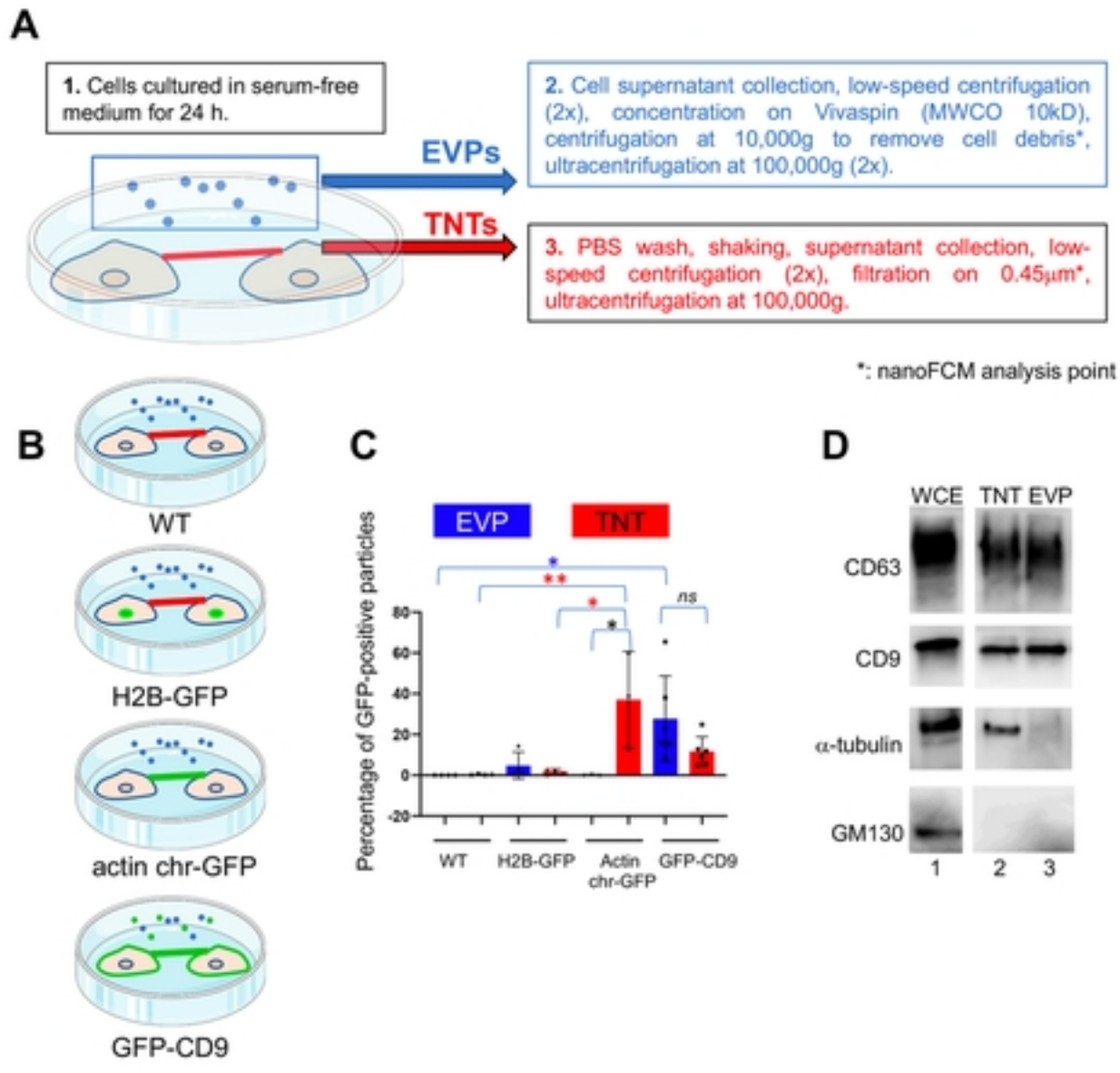
A
1. Cells cultured in serum-free medium for 24 h.
EVPs
2. Cell supernatant collection, low-speed centrifugation (2x), concentration on Vivaspin (MWCO 10kD), centrifugation at 10,000g to remove cell debris*, ultracentrifugation at 100,000g (2x).
TNTs
3. PBS wash, shaking, supernatant collection, low-speed centrifugation (2x), filtration on 0.45μm*, ultracentrifugation at 100,000g.
*: nanoFCM analysis point
B
WT
H2B-GFP
actin chr-GFP
GFP-CD9
C
EVP
TNT
Percentage of GFP-positive particles
ns
WT
H2B-GFP
Actin chr-GFP
GFP-CD9
D
WCE
TNT
EVP
CD63
CD9
α-tubulin
GM130
1
2
3

Figure 2

A

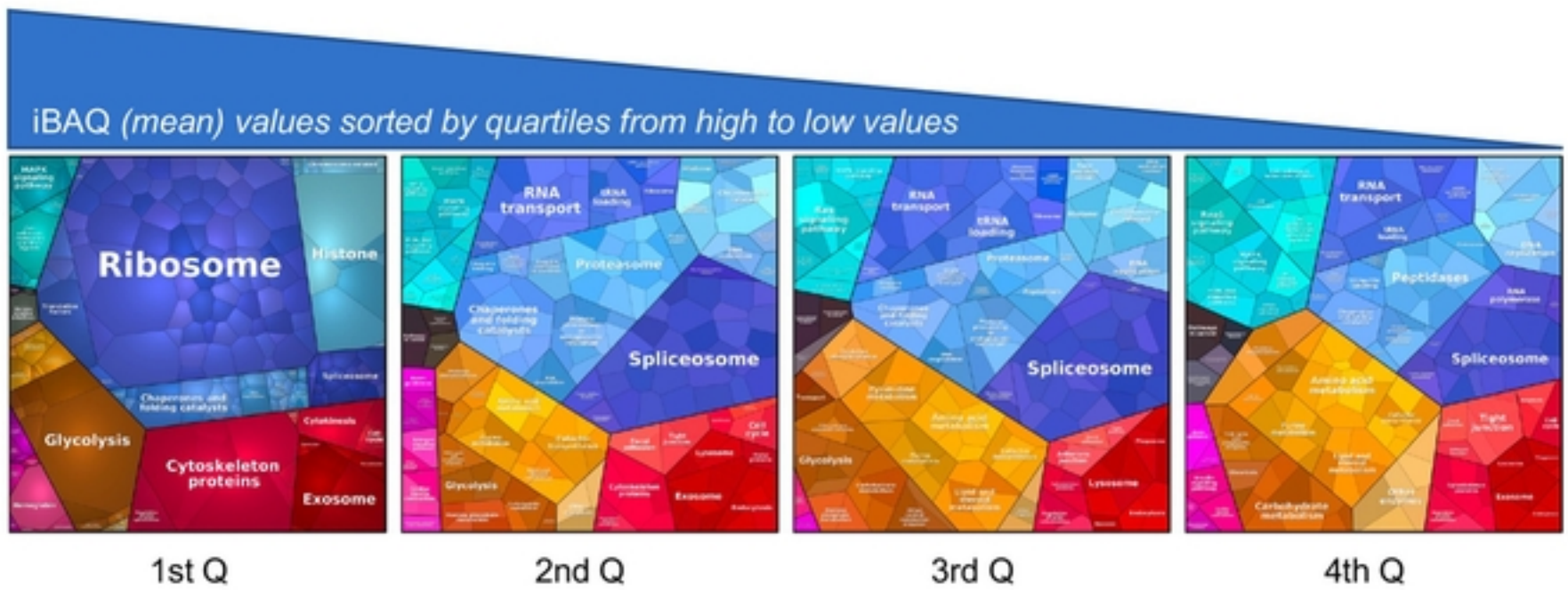

B

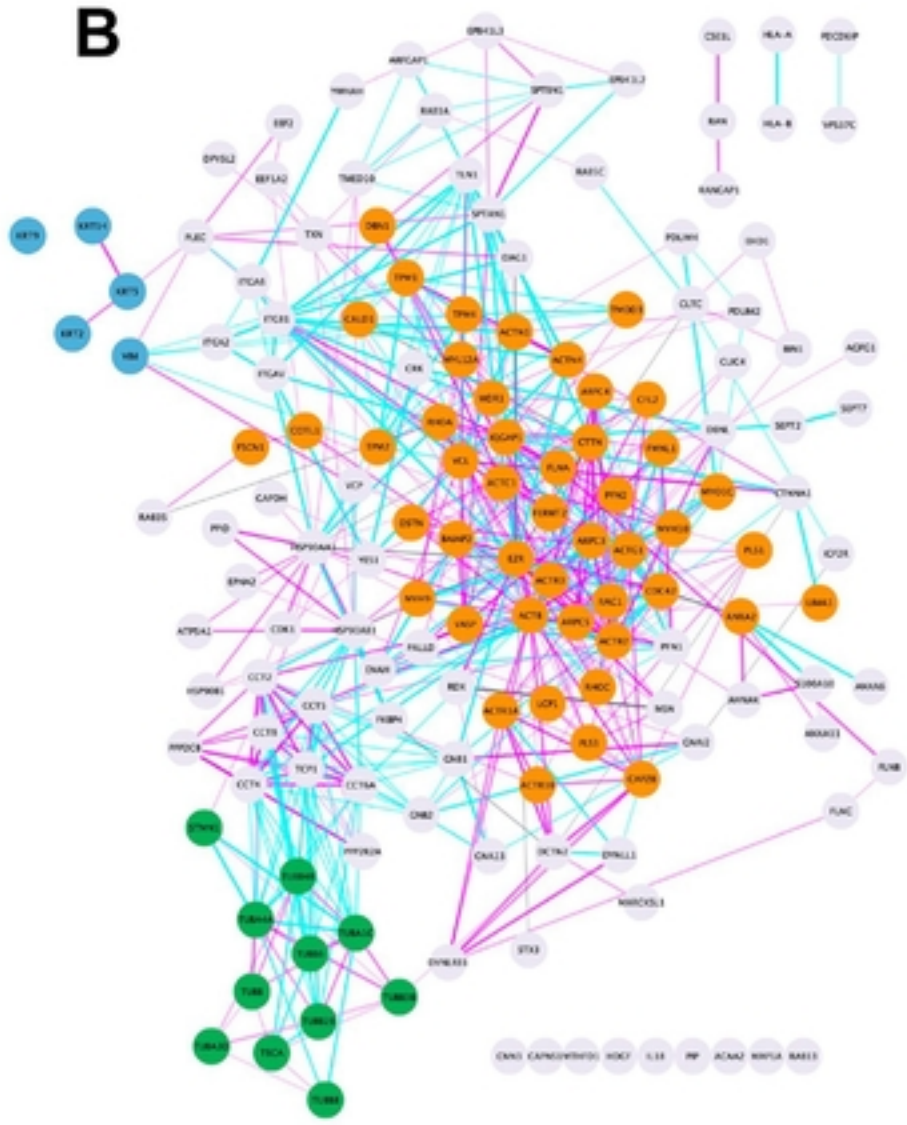

C

D

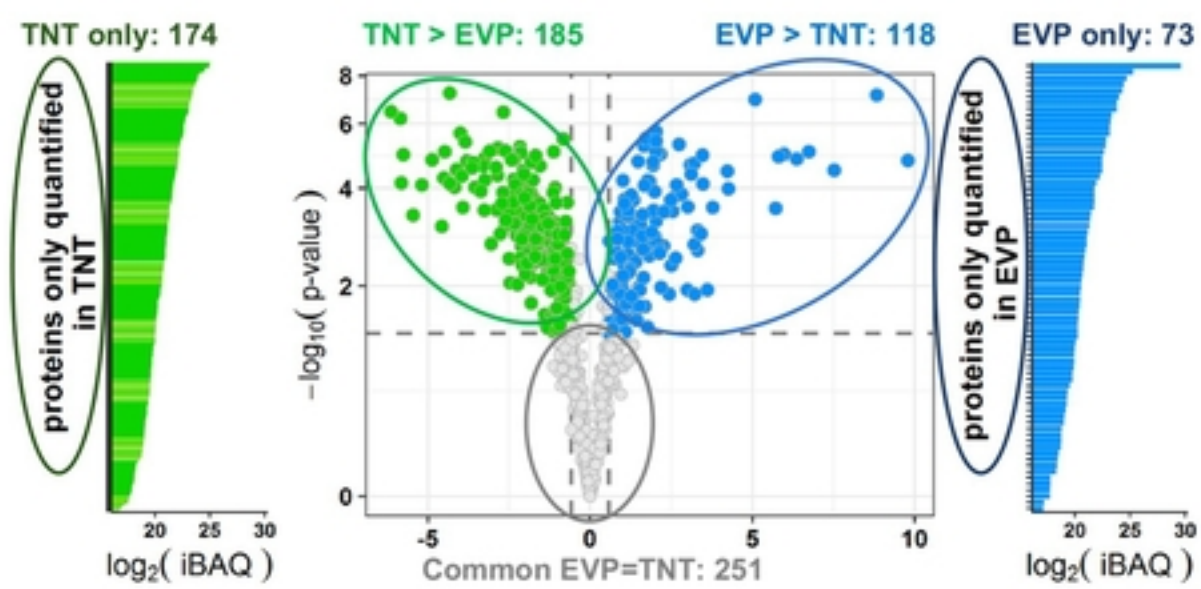

Figure 3

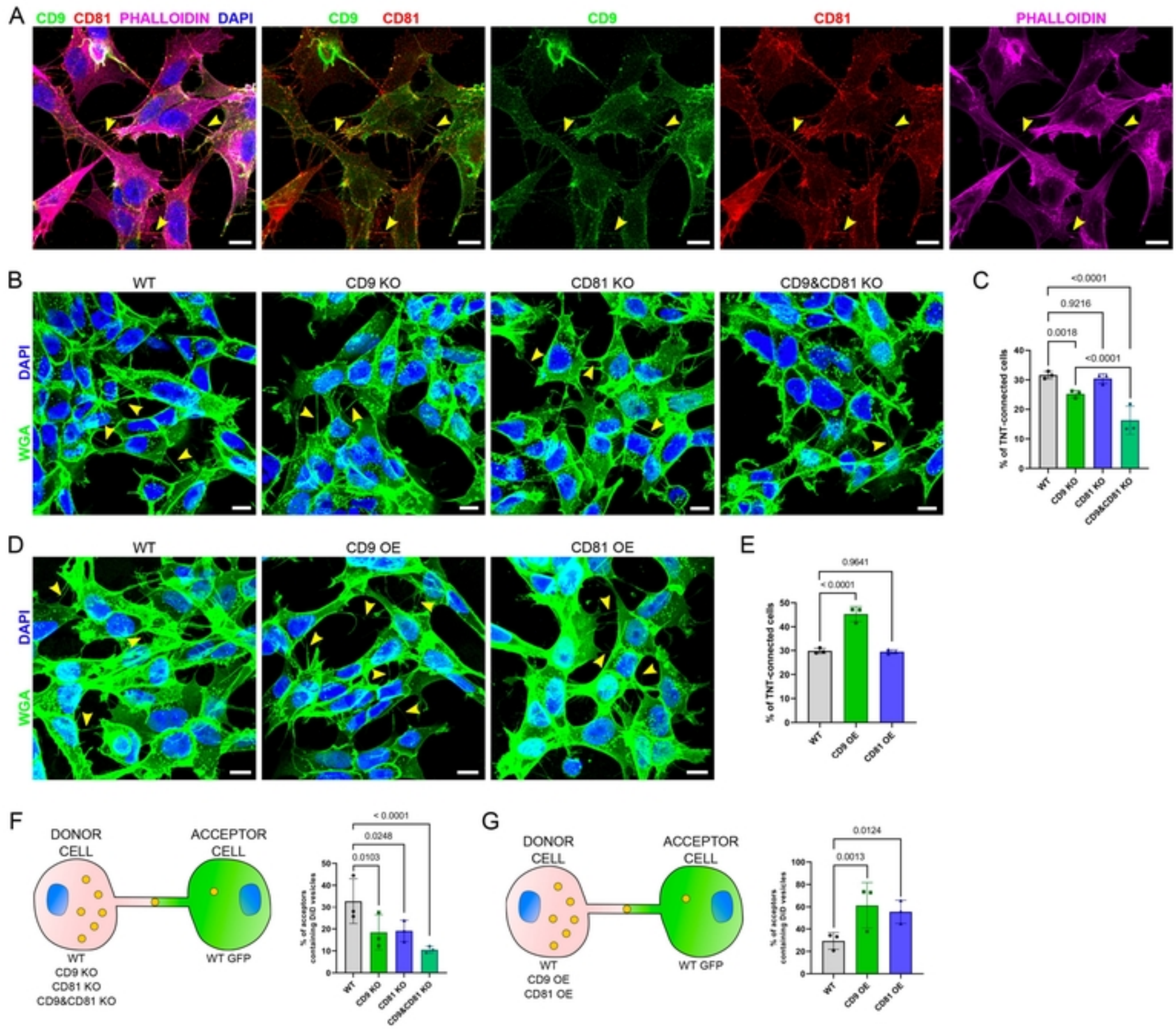
A
CD9 CD81 PHALLOIDIN DAPI
CD9 CD81
CD9
CD81
PHALLOIDIN
B
WT
CD9 KO
CD81 KO
CD9&CD81 KO
DAPI
WGA
C
<0.0001
0.9216
0.0018
<0.0001
% of TNT-connected cells
WT
CD9 KO
CD81 KO
CD9&CD81 KO
D
WT
CD9 OE
CD81 OE
DAPI
WGA
E
0.9641
< 0.0001
% of TNT-connected cells
WT
CD9 OE
CD81 OE
F
DONOR CELL
ACCEPTOR CELL
WT
CD9 KO
CD81 KO
CD9&CD81 KO
WT GFP
< 0.0001
0.0248
0.0103
% of acceptors containing DiD vesicles
WT
CD9 KO
CD81 KO
CD9&CD81 KO
G
DONOR CELL
ACCEPTOR CELL
WT
CD9 OE
CD81 OE
WT GFP
0.0124
0.0013
% of acceptors containing DiD vesicles
WT
CD9 OE
CD81 OE

Figure 4

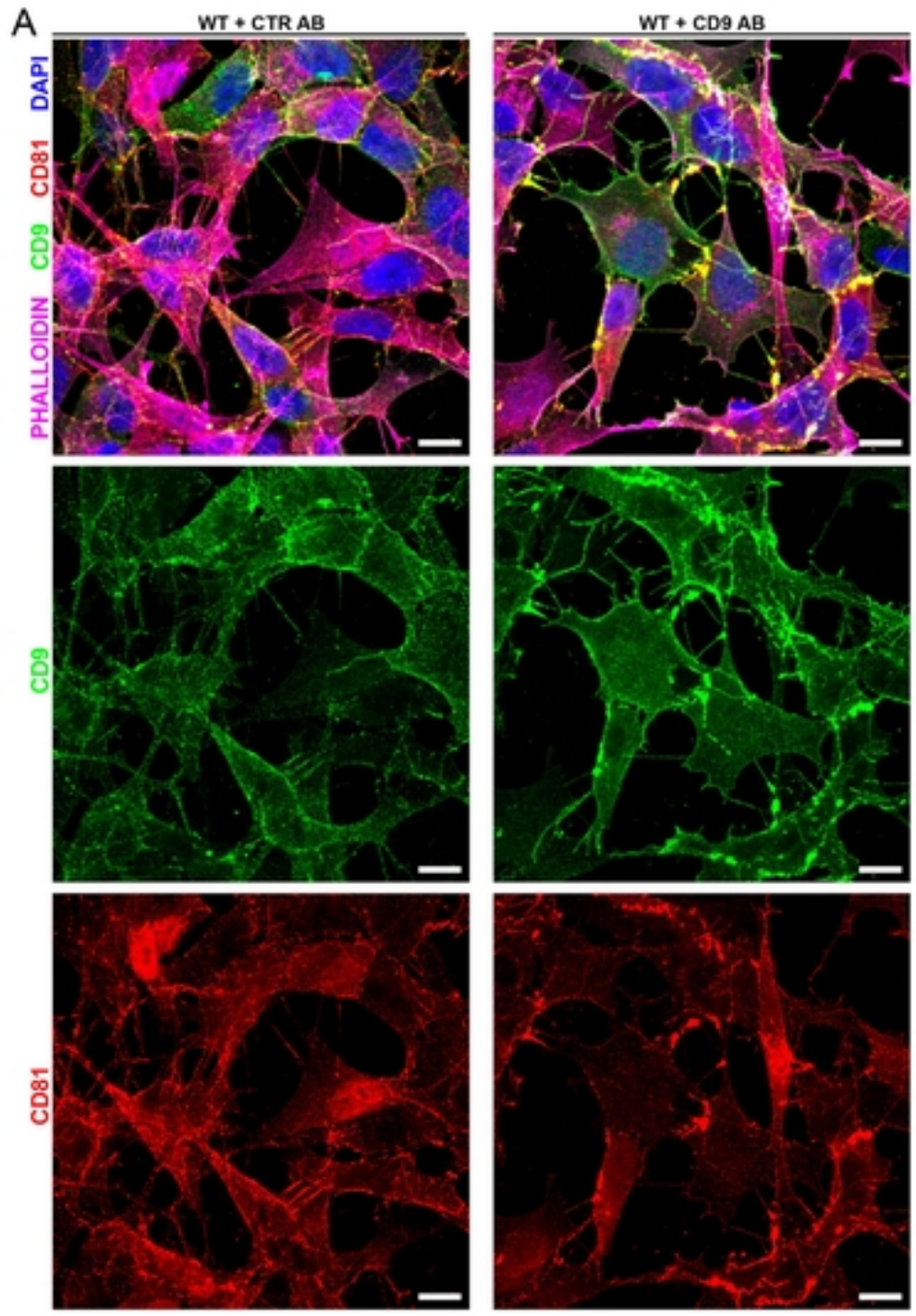
A
WT + CTR AB
WT + CD9 AB
DAPI
CD81
CD9
PHALLOIDIN
CD9
CD81

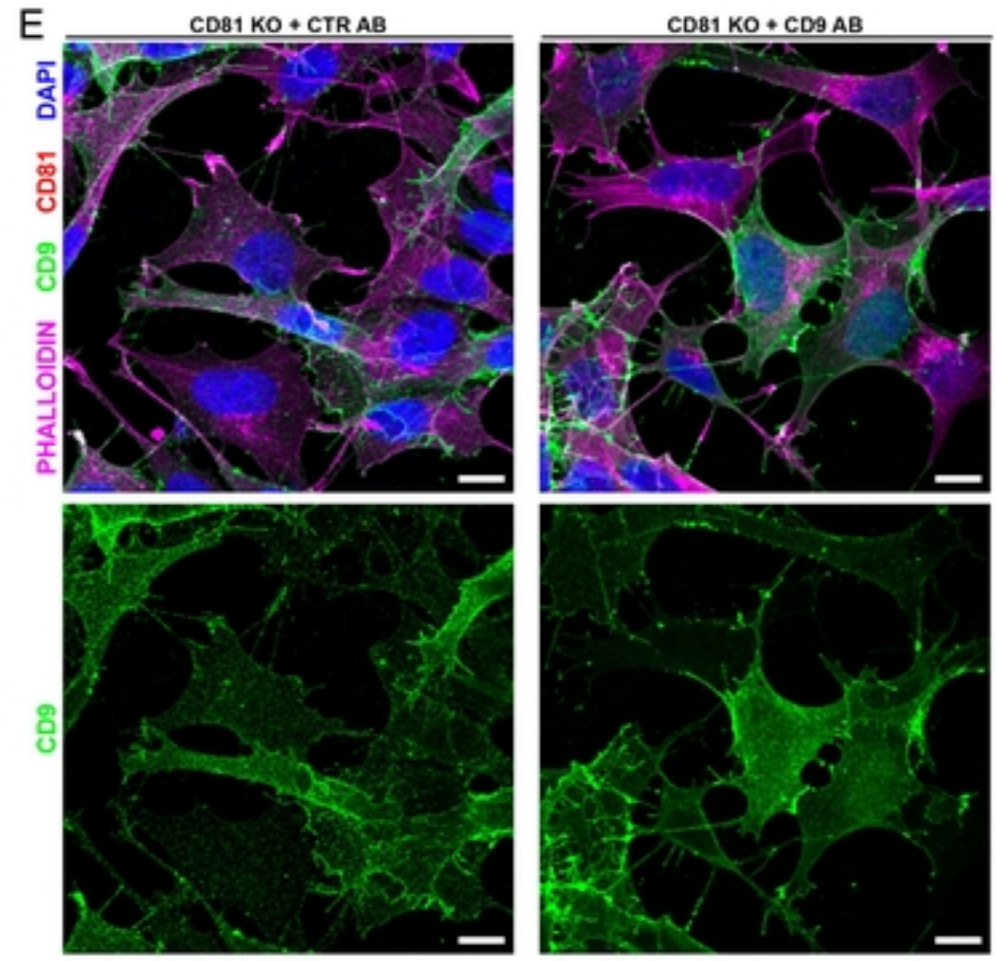
E
CD81 KO + CTR AB
CD81 KO + CD9 AB
DAPI
CD81
CD9
PHALLOIDIN
CD9

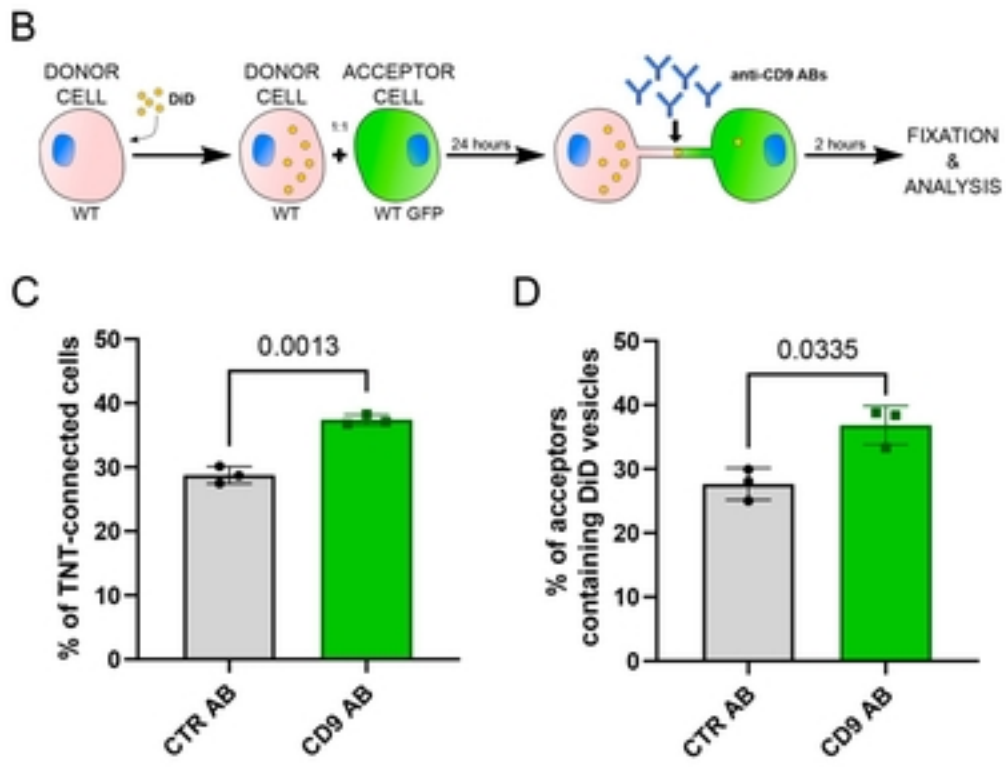
B
DONOR CELL
DiD
WT
DONOR CELL
ACCEPTOR CELL
1:1
WT
WT GFP
24 hours
anti-CD9 ABs
2 hours
FIXATION & ANALYSIS
C
% of TNT-connected cells
0.0013
CTR AB
CD9 AB
D
% of acceptors containing DiD vesicles
0.0335
CTR AB
CD9 AB

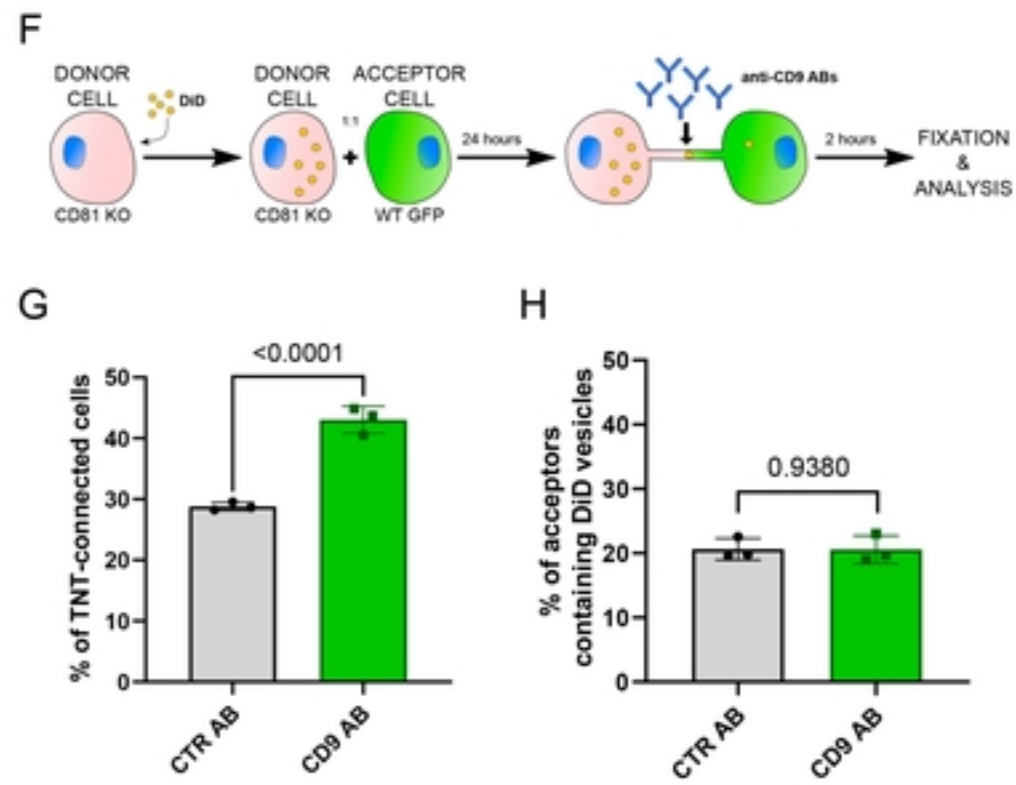
F
DONOR CELL
DiD
CD81 KO
DONOR CELL
ACCEPTOR CELL
1:1
CD81 KO
WT GFP
24 hours
anti-CD9 ABs
2 hours
FIXATION & ANALYSIS
G
% of TNT-connected cells
<0.0001
CTR AB
CD9 AB
H
% of acceptors containing DiD vesicles
0.9380
CTR AB
CD9 AB

Figure 5

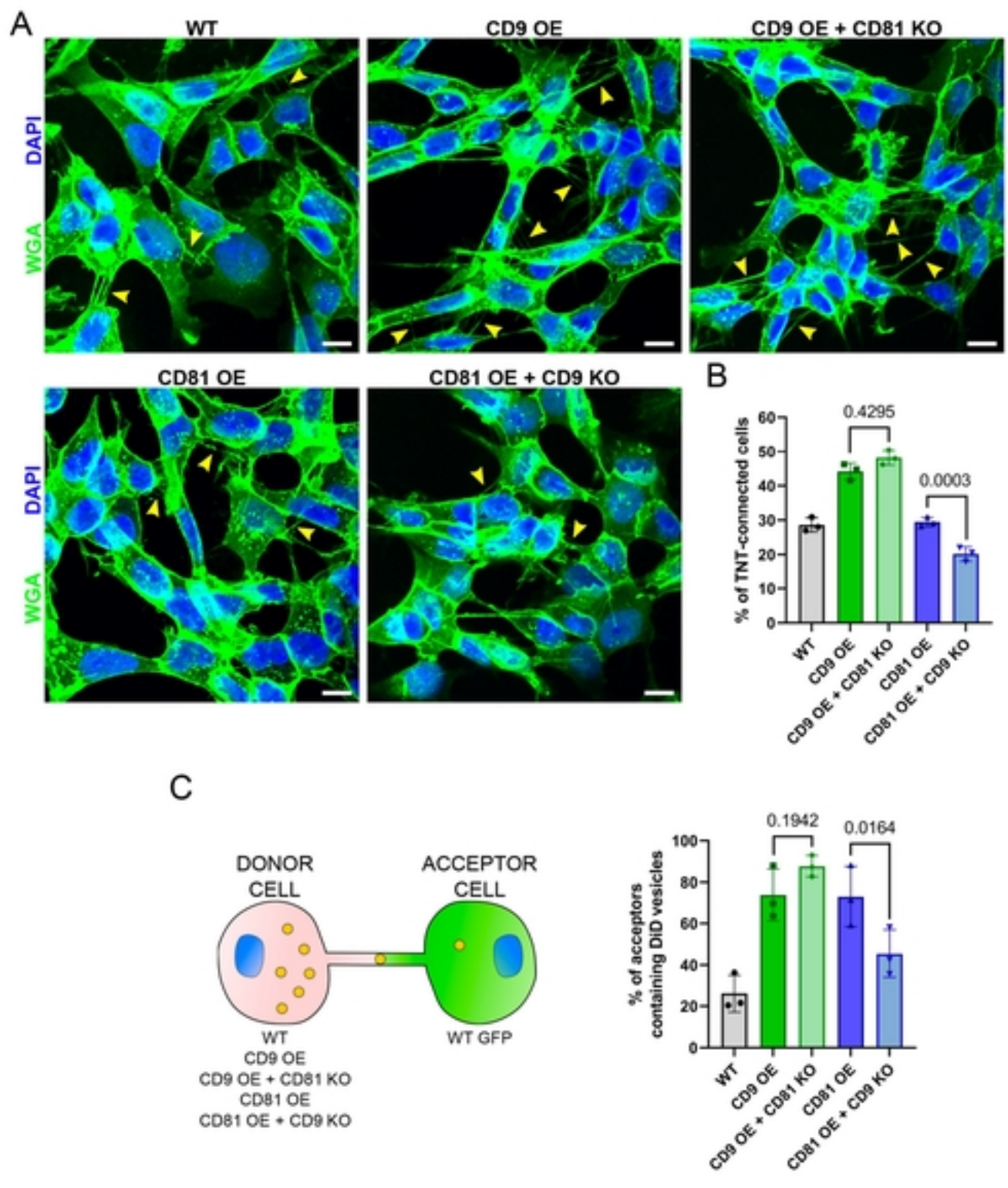
A
WT
CD9 OE
CD9 OE + CD81 KO
CD81 OE
CD81 OE + CD9 KO
DAPI
WGA
B
% of TNT-connected cells
0.4295
0.0003
WT
CD9 OE
CD9 OE + CD81 KO
CD81 OE
CD81 OE + CD9 KO
C
DONOR CELL
ACCEPTOR CELL
WT
CD9 OE
CD9 OE + CD81 KO
CD81 OE
CD81 OE + CD9 KO
WT GFP
% of acceptors containing DiD vesicles
0.1942
0.0164